UC Irvine
UC Irvine Previously Published Works

Title
Miles to go (mtgo) encodes FNDC3 proteins that interact with the chaperonin subunit CCT3 and are required for NMJ branching and growth in Drosophila.

Permalink
https://escholarship.org/uc/item/776483rk

Journal
Developmental biology, 445(1)

ISSN
0012-1606

Authors
Syed, Adeela
Lukacsovich, Tamás
Pomeroy, Miles
et al.

Publication Date
2019

DOI
10.1016/j.ydbio.2018.10.016

Peer reviewed

eScholarship.org Powered by the California Digital Library
University of California

Developmental Biology 445 (2019) 37–53

Contents lists available at ScienceDirect

Developmental Biology

journal homepage: www.elsevier.com/locate/developmentalbiology

Miles to go (*mtgo*) encodes FNDC3 proteins that interact with the chaperonin subunit CCT3 and are required for NMJ branching and growth in *Drosophila*

Adeela Syed[a], Tamás Lukacsovich[a,1], Miles Pomeroy[a], A. Jane Bardwell[a], Gentry Thomas Decker[b], Katrina G. Waymire[a], Judith Purcell[a], Weijian Huang[a], James Gui[a,2], Emily M. Padilla[a,2], Cindy Park[a,2], Antor Paul[a,2], Thai Bin T. Pham[a,2], Yanete Rodriguez[a,2], Stephen Wei[a,2], Shane Worthge[a,2], Ronak Zebarjedi[a,2], Bing Zhang[b], Lee Bardwell[a], J. Lawrence Marsh[a,*], Grant R. MacGregor[a,*]

[a] Department of Developmental and Cell Biology, School of Biological Sciences, University of California, Irvine, Irvine, CA 92697-2300, USA
[b] Division of Biological Sciences, University of Missouri, Columbia, MO 65211-7400, USA

ARTICLE INFO

Keywords:
MTGO
FNDC3
NMJ
CCT3
Drosophila
Neuronal

ABSTRACT

Analysis of mutants that affect formation and function of the *Drosophila* larval neuromuscular junction (NMJ) has provided valuable insight into genes required for neuronal branching and synaptic growth. We report that NMJ development in *Drosophila* requires both the *Drosophila* ortholog of *FNDC3* genes; *CG42389* (herein referred to as *miles to go; mtgo*), and *CCT3,* which encodes a chaperonin complex subunit. Loss of *mtgo* function causes late pupal lethality with most animals unable to escape the pupal case, while rare escapers exhibit an ataxic gait and reduced lifespan. NMJs in *mtgo* mutant larvae have dramatically reduced branching and growth and fewer synaptic boutons compared with control animals. Mutant larvae show normal locomotion but display an abnormal self-righting response and chemosensory deficits that suggest additional functions of *mtgo* within the nervous system. The pharate lethality in *mtgo* mutants can be rescued by both low-level pan- and neuronal-, but not muscle-specific expression of a *mtgo* transgene, supporting a neuronal-intrinsic requirement for *mtgo* in NMJ development. *Mtgo* encodes three similar proteins whose domain structure is most closely related to the vertebrate intracellular cytosolic membrane-anchored *fibronectin type-III domain-containing protein 3* (FNDC3) protein family. *Mtgo* physically and genetically interacts with *Drosophila CCT3*, which encodes a subunit of the TRiC/CCT chaperonin complex required for maturation of actin, tubulin and other substrates. *Drosophila* larvae heterozygous for a mutation in *CCT3* that reduces binding between CCT3 and MTGO also show abnormal NMJ development similar to that observed in *mtgo* null mutants. Hence, the intracellular FNDC3-ortholog MTGO and CCT3 can form a macromolecular complex, and are both required for NMJ development in *Drosophila*.

1. Introduction

Synaptic development and plasticity are sophisticated processes required for neuronal function. In *Drosophila*, synapses at the neuromuscular junction (NMJ) are glutamatergic and exhibit plasticity similar to that seen in excitatory glutamatergic synapses in the vertebrate central nervous system (CNS) (reviewed in Menon et al. (2013)). Consistent with this observation the *Drosophila* NMJ and vertebrate synapses share orthologs of several key proteins such as the scaffold protein Post-Synaptic Density protein 95 (PSD-95), which is structurally and functionally related to *Drosophila* discs large (DLG) (Guan et al., 1996; Lahey et al., 1994). *Drosophila's* relatively simple nervous system, combined with its powerful genetic tools, make it an excellent experimental system for use in identifying components required for synaptic development and plasticity in other species, and investigating their mechanisms of action (Bellen et al., 2010; Menon et al., 2013).

During *Drosophila* embryogenesis motoneuron axons exit the CNS in a stereotypical manner via discrete pathways (Ruiz-Canada and

* Corresponding authors.
E-mail addresses: jlmarsh@uci.edu (J.L. Marsh), gmacg@uci.edu (G.R. MacGregor).
[1] Present address: Brain Research Institute, University of Zurich, Switzerland.
[2] Authors made equal contribution.

https://doi.org/10.1016/j.ydbio.2018.10.016
Received 4 May 2018; Received in revised form 1 September 2018; Accepted 17 October 2018
Available online 25 October 2018
0012-1606/ © 2018 Elsevier Inc. All rights reserved.

Budnik, 2006). Each axon follows a genetically determined route to innervate a specific individual muscle fiber, or group of muscle fibers (Halpern et al., 1991; Landgraf et al., 1997; Sink and Whitington, 1991). Initial contact between the axon terminus and its target muscle stimulates clustering of various proteins (including DLG and glutamate receptors) on the post-synaptic side of the developing NMJ (Chen and Featherstone, 2005). The axon terminus then differentiates to form a pre-synaptic terminal. By the end of embryonic development the rudimentary NMJ is comprised of a small number of synaptic boutons, each of which contains active zones where synaptic transmission occurs, separated by thin neuritic processes (Yoshihara et al., 1997). During larval development the muscle fibers increase dramatically in size. To maintain adequate synaptic stimulus at the NMJ, the motoneuron ending also grows. By the end of larval development both the number of boutons and active zones per bouton can increase by 10-fold resulting in between 20 and 40 active zones per bouton (Atwood et al., 1993; Schuster et al., 1996). Expansion of the larval NMJ occurs via growth of the motoneuron endplate through elongation of neurites, formation of new branches (arborization) and addition and expansion of new boutons (Zito et al., 1999).

Much of the current understanding of NMJ growth and branching in *Drosophila* comes from analysis of mutants that affect this process (reviewed in Menon et al. (2013)). These studies have demonstrated that a diverse collection of proteins is required for NMJ growth and branching including proteins with functions in cell adhesion, cell polarity, signaling, trafficking, protein modification and turnover, and DNA transcription (reviewed in Menon et al. (2013)). Many of these proteins affect NMJ growth in a dose-dependent manner that may influence synaptic plasticity. Here, we identify the *Drosophila* gene that encodes an ortholog of vertebrate FNDC3 proteins and show that both it and the chaperonin subunit CCT3 are also required for NMJ development in *Drosophila*.

FNDC3 proteins are composed of an N-terminal proline-rich region (PRR), eight or nine fibronectin type-III (FN3) domains, and a hydrophobic C-terminus membrane anchoring domain (Carrouel et al., 2008; Obholz et al., 2006; Tominaga et al., 2004). In vertebrates, FNDC3 proteins are intracellular cytosolic tail-anchored (TA) ER-membrane-localized proteins whose membrane location appears necessary for their activity (Cai et al., 2012; Lin et al., 2016). Analyses of *Fndc3* genes in mice and humans indicate that FNDC3 proteins have broad functions in development and homeostasis, including maintenance of spermatid intercellular bridges and spermatid-Sertoli cell adhesion during spermatogenesis (Obholz et al., 2006), craniofacial, skeletal and lung development (Cao et al., 2016; Kishimoto et al., 2013, 2011; Nishizuka et al., 2009) and adipogenesis (Nishizuka et al., 2009; Tominaga et al., 2004). In addition, amplification or increased expression of *FNDC3B* is associated with different cancers including glioma and glioblastoma (Stangeland et al., 2015) and hepatocellular carcinoma (Cai et al., 2012; Chen et al., 2010; Lin et al., 2016). How FNDC3 proteins function mechanistically in each of these processes is not yet fully understood.

Analyzing the function of orthologs of mammalian genes in a genetically tractable and diverse species such as *Drosophila* is a powerful way to identify conserved gene functions and to understand how their encoded proteins work (Yamamoto et al., 2014). Here, we identify *mtgo* as the *Drosophila* gene that encodes orthologs of vertebrate FNDC3 proteins (Obholz et al., 2006; Tominaga et al., 2004). We show that *mtgo* is required in neurons for terminal axon arborization and growth at the NMJ during larval development and that homozygous null mutation of *mtgo* results in late pupal lethality. *Mtgo* interacts both genetically and physically with *CCT3* (previously known as *vine)* (Ghabrial et al., 2011), which encodes a subunit of the TRiC/CCT chaperonin complex (Frydman et al., 1992; Gao et al., 1992; Lopez et al., 2015; Willison et al., 1986; Yaffe et al., 1992). Significantly, heterozygous mutant *CCT3* larvae display similar NMJ branching defects. Hence, MTGO functions as a membrane-anchored component of a cytosolic juxta-membrane molecular complex that includes CCT3. In *Drosophila*, *mtgo* is required for multiple processes including growth and branching of the NMJ, normal olfactory behavior and righting response during larval development.

2. Materials and methods

2.1. Identification and sequence comparison of orthologs of vertebrate FNDC3 proteins

Orthologs of *Fndc3* genes in *D. melanogaster* were identified using the Simple Modular Architecture Research Tool (SMART; http://smart.embl-heidelberg.de) to search databases for proteins having the same domain architecture found in mammalian FNDC3 proteins. Comparison of the fibronectin type III (FN3) domains encoded by *mtgo* (*CG42389)* with all other FN3 domain-containing proteins in the *D. melanogaster* genome was performed using the Basic Local Alignment Search Tool (BLAST). Regions of homology between FNDC3 proteins were identified using the CLUSTALW algorithm within the MegAlign program within the DNASTAR Navigator Suite v 12.0 (DNASTAR Inc, Madison, WI).

2.2. Drosophila stocks, germline transformations and crosses performed

Fly stocks were maintained at 22 °C on standard cornmeal-molasses medium. Wild-type control flies were Canton S or YW. Intercrosses between transgenic flies were conducted using 5–10 virgin females of one strain placed in a vial with 2–4 males of another strain at 25 °C. Except where indicated, all stocks were obtained from the Bloomington Drosophila Stock Center (Bloomington, IN). Strains of flies used were as follows. *Mtgo* alleles *e02963* (stock #18101), *MI11367* (#56312), *KG00841*, (#12961), *KG03432* (#13784), *MI00732* (#32693), *EP1224* (#16998), *MI05370* (#55422), *A043* (#16019), and *MI01789* (#32782). Df(2L)Exel7066 (stock #7833) has a single deficiency on 2L between 36A1 and 36A12 (with breakpoints 16,457,328 and 16,727,482) that deletes 29 genes including *mtgo*. Df(2L)ED1109 (stock # 8945) has a single deficiency on 2L between 36A3 and 36A10 (with breakpoints 16,520,606 and 6685,396) that deletes 12 genes including *mtgo*. For rescue experiments *elav* > Gal4 (stock #458), *Arm* > Gal4 ChrIII (stock#1561), *Mef2* > Gal4 (stocks #27390; 26882), *c179* > Gal4 (stock #6450) and *actin* > Gal4 (P{Act5C-GAL4}17bFO3, (Ito et al., 1997) a generous gift of Daisuke Yamamoto, Tohoku University, Sendai, Japan) were used. Flies with the $mtgo^{CPTI001586}$ allele (stock #115175) (Lowe et al., 2014) containing an in-frame Enhanced Yellow Fluorescence Protein (EYFP) gene-trap insertion in intron 3 of *mtgo-RF* (Fig. 1) were obtained from the Drosophila Genomics and Genetic Resources (DGGR), Kyoto Institute of Technology, Japan. *CyO-GFP* was used in crosses when it was necessary to identify mutant larva. Fly stocks carrying a missense mutation (G297D) in the *CCT3* gene ($CCT3^{512}$) (Ghabrial et al., 2011) were the generous gift of Amin Ghabrial (Columbia University Medical Center, NY). NMJs were examined in btl-Gal4,UAS-GFP (2); FRT2A,FRT82B $CCT3^{512}$/TM3, Sb, Tub-Gal80 non-GFP (*i.e.* heterozygous for $CCT3^{512}$) larvae. To verify that the effects observed were attributable to the $CCT3^{512}$ mutation, NMJs were also examined from larvae having a genomic rescue construct (y w FLP^{122}; p{*CCT3*}; FRT2A,FRT82B $CCT3^{512}$/Df(3R)*CCT3 2*) and were found to be fully rescued, supporting that the NMJ phenotype was not due to a second-site mutation. To test for genetic interaction between *CCT3* and *mtgo*, or *wit* and *mtgo*, flies were crossed to produce *w[1118];* PBac{RB} CG42389[e02963]/ actGFP(#52665), which were crossed to btl-Gal4,UAS-GFP (2); FRT2A,FRT82B $CCT3^{512}$/TM3 Sb, Tub-Gal80 or *bw;* wit^{B11} *st*/ TM6B, *Tb* (Marques et al., 2002; Marqués et al., 2003) as a control.

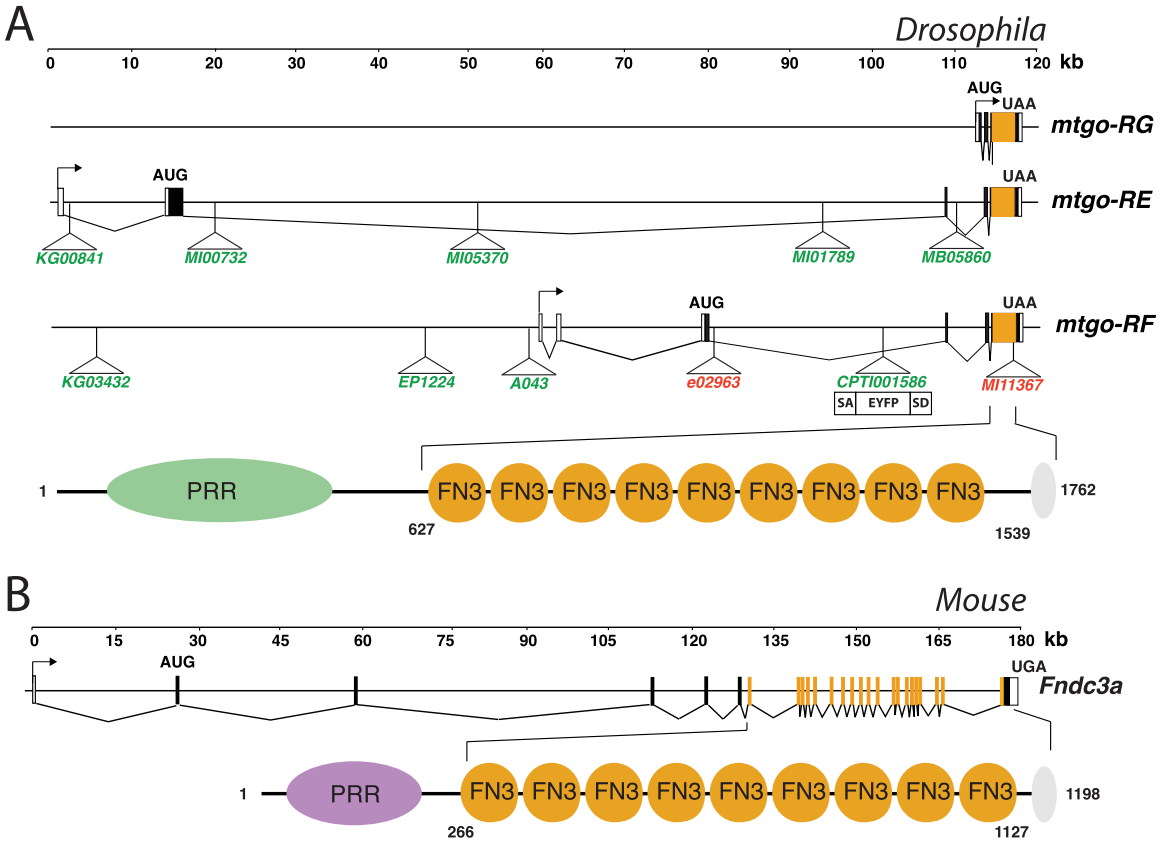

Fig. 1. Transcripts encoded by *mtgo* (*CG42389*), the *Drosophila* ortholog of vertebrate *FNDC3* genes, the location of exons encoding fibronectin type III (FN3) domains, and *Drosophila* mutant alleles analyzed in this study. (A) The location of the exons encoded by three transcripts (*-RE*, *-RF* and *-RG*) produced by the *mtgo* (*CG42389*) locus in *D. melanogaster*. Transcriptional start sites are denoted by horizontal arrows; non-coding regions of exons by open boxes; coding regions of exons by filled boxes. The location of the translational start (AUG) and stop (UAA) site for each transcript is indicated. Shown below the physical map is the structure of the protein encoded by the *mtgo-RF* transcript including the N-terminal proline rich region (PRR), the nine FN3 domains and the hydrophobic C-terminal tail-anchoring (TA) sequence (grey oval). All three *mtgo* transcripts encode proteins containing FN3 domains encoded by the orange colored region within the last exon, and end with a C-terminal TA sequence. For clarity, the genomic location for the P element/PBacs/gene-trap insertions in mutant alleles analyzed in this study are arbitrarily located on the *–RE* and *–RF* transcripts. Alleles whose names are in green have no obvious mutant phenotype when *in trans* to a deficiency allele, while the two alleles in red are lethal as homozygotes, and *in trans*, either to a deficiency or to each other. The site of insertion of the *piggyBac* in the $mtgo^{e02963}$ allele is 49 bp 3′ to exon 3 of *mtgo-RF* and predominantly affects the -RF isoform, while the location of the $Mi\{MIC\}mtgo^{MI11367}$ insertion that affects all three transcripts is within the last exon. The location of the SA-EYFP-SD cassette in the $mtgo^{CPTI001586}$ allele (i.e. MTGO-EYFP) used to image MTGO expression in larvae is indicated. (B) An example of the exon structure of *Fndc3* genes in vertebrates. In contrast to *mtgo*, the nine FN3 domains in mouse *Fndc3a* are encoded by 20 exons (colored orange) instead of a single exon. The N-terminal PRR and hydrophobic TA terminus (grey oval) are indicated. The different color of the mouse PRR denotes the general lack of sequence similarity between the *Drosophila* PRR and the PRR's of the vertebrate clade (Supplementary Table 2). Numbers indicate the amino acids in mouse FNDC3A (1198 aa) and the protein encoded by *mtgo-RF* (1762 aa) and also denote the start and end of the FN3 domains. Note the different scales used to represent the size of each gene. The relative location of exons was determined from Ensembl databases - Ensembl metazoa release 22 (April 2014) for *Drosophila*; Ensembl release 75 (Feb 2014) for mouse.

2.3. Characterization of mutant alleles of mtgo

Ten uncharacterized insertion alleles of *mtgo* were analyzed (Fig. 1). Three alleles ($mtgo^{e02963}$, $Mi\{MIC\}mtgo^{MI01789}$ and $Mi\{MIC\}mtgo^{MI11367}$) are held as heterozygotes over a balancer. The $mtgo^{e02963}$ allele contains a *piggyBac* inserted in intron 3, 49 bp downstream of the first coding exon of the *RF* transcript while the $Mi\{MIC\}mtgo^{MI01789}$ allele contains a MiMIC insert (Venken et al., 2011) within intron 3. The $Mi\{MIC\}mtgo^{MI11367}$ allele also contains a MiMIC insert within the final exon common to all isoforms, which disrupts the last FN3 domain encoded by *mtgo*. Initial observations from *inter se* crosses indicated recessive lethality of all 3 chromosomes. To confirm the mutant phenotypes were due to the insertion in the *mtgo* locus and not to second-site mutations, flies carrying each of the alleles were crossed with animals carrying *Df(2L) Exel7066*, which deletes 29 genes on chromosome 2L including the *mtgo* locus. Animals heterozygous for either $mtgo^{e02963}$ or $Mi\{MIC\}mtgo^{MI11367}$ with *Df(2L)Exel7066* were lethal, supporting that the mutant phenotypes observed are likely due to the insertion allele. However, animals containing the $Mi\{MIC\}mtgo^{MI01789}$ allele *in trans* to the *Df* were viable as adults, suggesting its lethality when homozygous is due to a second-site mutation located outside of the 29-gene domain defined by the deficiency. To confirm allelism of $mtgo^{e02963}$ and $mtgo^{MI11367}$, complementation was tested by crossing $mtgo^{e02963}$ /*CyO* to $mtgo^{MI11367}$/SM6a (Cy^{1}). CyO/SM6a animals are lethal. Only 11 non-curly wing (i.e. $mtgo^{e02963}/mtgo^{MI11367}$ heteroallelic) animals were found in 654 F1 flies (~3.4% of expected) confirming the allelism of these two insertional mutations. An additional seven insertional alleles provided as homozygotes from the Bloomington stock center were also tested (Fig. 1). These alleles produced viable and fertile adults over *Df(2L)Exel7066* and were not studied further.

2.4. Determination of lethal phase

The lethal phase of *mtgo* mutants was determined using two approaches. First, 100 $mtgo^{e02963}$ homozygote and $mtgo^{e02963}$/*CyO-GFP* heterozygote first-instar larvae were collected and the number of viable animals of each genotype recorded at late-larval, pupal, pharate, and adult stages. The second method involved crossing $mtgo^{e02963}$ or $mtgo^{MI11367}$/*CyO-GFP* animals and scoring at L1, L3 and as adults for presence or absence of the *CyO-GFP* balancer (N > 400).

2.5. Analysis of transcripts affected by PBac insertion in the *mtgo*^{e02963} allele

Animals (larvae or adults) were selected from intercross of heterozygous *mtgo*^{e02963}*/CyO-GFP* balanced flies, with homozygous *mtgo*^{e02963} animals identified by the absence of GFP in larvae, or by phenotype in rare adult escapers. Wild-type control animals were collected from separate crosses. RNA and cDNA were prepared from biological triplicates. For quantitative RT-PCR, total RNA was prepared from frozen larvae or adults by grinding samples with a motorized plastic pestle in TRIzol (ThermoFisher Scientific, Carlsbad, CA) for 1 min followed by processing using the manufacturer's recommendations. RNA was reverse transcribed (RT) with random primers using SuperScript III (ThermoFisher Scientific, Carlsbad, CA) or Fermentas Maxima Universal First Strand cDNA Synthesis Kit #K1661 (ThermoFisher Scientific, Waltham, MA) following the manufacturer's protocol. Reaction products were diluted with water and quantitative PCR (qPCR) performed using SYBR Green on a DNA Engine Continuous Fluorescence Detection System (MJ Research, Reno, NV). Primers used for RT and qPCR and their target sequences within the *mtgo* locus are listed in Supplemental Fig. 2. The quantity of an individual isoform of *mtgo* cDNA was normalized to the quantity of cDNA for *ribosomal protein 49* (*rp49)* (LaLonde et al., 2006) using a standard $\Delta\Delta C_T$ calculation (Livak and Schmittgen, 2001). Preliminary experiments using dilution of template verified that the efficiency of amplification of each target was as predicted. The *mtgo* locus produces three transcripts; *mtgo-RE*, *-RF* and *-RG* (Fig. 1). Although FlyBase (FB2017_04, released August 22, 2017) predicts the existence of a fourth transcript (*-RH*) comprised of *-RF* plus an additional exon, we were unable to detect the *-RH* isoform by RT-PCR using cDNA from larval or adult animals. This isoform might be expressed in embryos, which were not tested. Quantitative RT-PCR of the *-RE* and *-RF* transcripts in wild-type versus heterozygous and homozygote *mtgo*^{e02963} animals (n = 3 biological replicates for each genotype) showed that the *-RF* transcript is reduced to 23.2% ± 1.9% in heterozygote, and to 0.01% ± 0% in homozygote animals normalized to wild-type. In contrast, the quantity of the longer *-RE* transcript which contains the *mtgo*^{e02963} PBac insertion in the middle of a 92.8 kb intron was relatively mildly affected (93.1% ± 6.3% in heterozygotes and 64.2% ± 4.0% in homozygotes normalized to wild-type). Separate comparison of the quantity of *-RG* transcripts in adult wild-type, heterozygous and homozygous mutant *mtgo*^{e02963} flies showed the level to be grossly normal in *mtgo*^{e02963} mutant animals. Hence, the *mtgo*^{e02963} allele results in loss of the *-RF*, but not the *-RE* and *-RG* transcripts from the *mtgo* locus.

2.6. DNA constructs and production of transgenic animals

The *UAS > mtgo-RF* transgene was constructed by cloning a full-length cDNA coding sequence for the *mtgo-RF* transcript into the pUASTattB vector (Bischof et al., 2007). Complementary DNAs (*mtgo-RF* isoform was RE04201; *mtgo-RG* isoform LD30602) were obtained from the Drosophila Genome Research Center (DGRC; Bloomington, Indiana). The clone used for the *RF* isoform (RE04201) contained a frameshift mutation that was corrected. More recently, a non-mutated *RF* cDNA (FI20237) has appeared in the DGRC collection. Germline transformations were performed by injection using standard methods into the phiC31 targeting stock *yw* hs-flp; AttP-zh86Fb RFP; vas-ϕ-zh102D to generate inserts at 86Fb (Bischof et al., 2007).

2.7. Immunofluorescence analysis of NMJs

NMJs were analyzed in muscles 4, 5, 6/7, 8, and 15/16 of abdominal segment 2 (A2) of wandering third-instar larvae. Larvae were heat shocked at 85 °C for 15 s to prevent muscle contraction. Animals were dissected in 1x phosphate buffered saline (PBS) (10 mM PO_4, 137 mM NaCl, and 2.7 mM KCl pH 7.4), fixed in 0.25 ml 4% formaldehyde in PBS at room temperature for 20 min followed by three 15 min washes in 1x PBS. Samples were washed a final time for 15 min in PBT (PBS with 0.1% Triton-X-100) prior to adding primary antibodies. To analyze Futsch-positive microtubule "loops" and "splays", larvae were directly dissected in HL3.1 Ca^{2+}-free buffer (70 mM NaCl, 5 mM KCl, 4 mM $MgCl_2$, 10 mM $NaHCO_3$, 5 mM trehalose, 115 mM sucrose, 5 mM HEPES, pH 7.4) and fixed for 30 min in Bouin's fixative (Sherwood et al., 2004). Primary monoclonal antibodies from Developmental Studies Hybridoma Bank (DSHB, University of Iowa, IA) were added using the following dilutions: mouse anti-DLG (4F3) 1:100; mouse anti-Futsch (22C10), 1:50. Cy5-conjugated goat anti-HRP was used at 1:500 (Jackson ImmunoResearch Laboratories, Inc., West Grove, PA). Alexa Fluor 488- conjugated secondary antibodies (Molecular Probes/ ThermoFisher Scientific, Carlsbad, CA) were each used at 1:100. All samples were mounted with Vectashield (Vector Laboratories, Burlingame, CA). In each experiment, samples of different genotypes were processed concurrently and imaged under identical settings, with exceptions stated.

2.8. Quantitation of bouton size, number and length of branching within the NMJ

Although boutons were quantified in NMJ from muscle 6/7, similar phenotypes were observed at other NMJs. Segment A2 was analyzed for bouton number and muscle area. Unless stated, at least six NMJs of each genotype were analyzed. Confocal images were acquired using Plan-Apo 20x/0.8NA or Plan-Apo 63x/1.4NA oil differential interference contrast objectives on an Axio-observer Z1 coupled to a Zeiss LSM 780 confocal microscope (Carl Zeiss Inc., Thornwood, NY). Analysis of homozygous CPTI001586 larvae with the EYFP gene-trap allele of *mtgo* (Lowe et al., 2014) was performed in photon-counting mode using a GaAsP detector. Images were analyzed using Zen 2011 (Carl Zeiss Inc.) and Volocity (Perkin-Elmer, Waltham, MA) and compiled using Adobe Photoshop CS4 (Adobe Inc., San Jose, CA) software. Branch points were defined as any branch of two or more boutons from the primary nerve terminal and any subsequent branches from these secondary branches. Branch length was determined using Zen 2011 software, where arbors of primary and secondary branch nerve terminals were measured starting at the first bouton or branch point. A bouton was defined as a synaptic varicosity (swelling) compared with adjacent axonal segments in tissues labeled with the presynaptic marker anti-horseradish peroxidase (Jan and Jan, 1982) and the postsynaptic marker, anti-Discs Large (anti-DLG) (Parnas et al., 2001). Boutons were quantified using maximum projections of Z-stacks that originated above and ended below the NMJ. Type Ib and Type Is boutons were identified based on shape using anti-HRP (neuronal membrane) and anti-DLG staining, which identifies the post-synaptic muscle membrane surrounding presynaptic motor axon terminals. Anti-DLG staining is abundant around type Ib boutons and is present at lower levels surrounding type Is boutons (Lahey et al., 1994). Ghost boutons were defined as a varicosity adjacent to a nerve branch that stained with HRP but not anti-DLG (Ataman et al., 2006). The numbers of independent samples analyzed are indicated in the figure legends. Statistical analysis was performed using Prism 5.0 f (GraphPad Software Inc., La Jolla, CA). Comparison of different categories was performed using one-way ANOVA with Tukey's multiple comparison test as stated in text.

2.9. Behavioral Analyses

Self-righting behavior was performed by rolling individual larvae onto their dorsum as described (Bodily et al., 2001). Initiation of righting behavior was defined as when the larva began to move after being rolled upside down. Righting behavior was considered completed

when the larva was fully upright. The time to both initiate righting and to complete righting were recorded. Five independent larvae were analyzed for each trial, and trials were repeated three times with different sets of animals. **Tactile stimulation** - sense of touch was analyzed using a simple withdrawal-response test (Bodily et al., 2001). Larvae were touched on the flank using a small plastic pipette tip and the response recorded. Data was expressed as percentage withdrawal (i.e. turning and migration away from stimulus) following stimulation. **Light avoidance** was measured as described (Dettman et al., 2001; Mazzoni et al., 2005). Briefly, early third-instar larvae were placed on 1% agarose plates. Half the bottom and the sides of each plate were covered in black electrical tape and placed on a light box. Ten larvae were placed on the plate for 15 min and the number of larvae in the light or dark half was recorded every 30 s **Olfaction** was tested using a 1:1000 dilution of ethyl acetate as described (Khurana and Siddiqi, 2013). Fifty wandering-stage larvae were washed in distilled water to remove food, dried briefly on filter paper then placed into the center of a 100 mm petri-dish containing 20 ul of ethyl-acetate dispensed on two 10 mm diameter filter discs placed diametrically opposite each other in the dish in areas defined as 'odor zones'. Larvae were allowed to wander for two min, then the number of larvae in each odor zone was recorded. The experiment was conducted three independent times with new cohorts of larvae. **Pausing and head sweep during locomotion** – a single 'pause' was defined as a temporary arrest in crawling followed by body flexing (head rearing) and sweeping (Wang et al., 1997). Pauses were quantified by placing individual wandering third-instar larvae animals on an agar plate lacking fruit juice and recording the number of independent pauses per minute over a five-minute test period. The numbers of independent samples analyzed are indicated in the figure legends. Statistical analysis was performed using Prism 5.0 f. Comparison of different categories was performed using either unpaired *t*-test, or Mann-Whitney test.

2.10. Electrophysiology of NMJ

Electrophysiology was analyzed in heterozygous $mtgo^{e02963}$ and $mtgo^{e02963}$/Df(2L)ED1109 larvae recovered as non-GFP F1 larvae from a Df(2L)ED1109 /CyO-GFP X $mtgo^{e02963}$/CyO-GFP cross. Recordings of evoked excitatory junctional potentials (EJP) and mini EJP (mEJP) were performed as described (Kim et al., 2012) with the following modifications. Briefly, wandering third-instar larvae were dissected in physiological saline HL-3 saline (Stewart et al., 1994), washed, and immersed in HL-3 containing 0.8 mM Ca^{2+}. Nerve roots were cut near the exiting site of the ventral nerve cord and intracellular recordings were made from muscle 6. Muscle synaptic potentials were recorded using an Axon Clamp 2B amplifier (Axon Instruments/ Molecular Devices, Sunnyvale, CA) and pClamp software (Molecular Devices, Sunnyvale, CA). Following motor-nerve stimulation with a suction electrode (100 msec, 5 V), evoked EJPs were recorded. Three to five EJPs evoked by low frequency of stimulation (0.1 Hz) were averaged. For mini recordings, 1 mM tetrodotoxin was added to prevent unwanted evoked release (Stewart et al., 1994). To calculate mEJP mean amplitudes, 50–100 events from each muscle were measured and averaged using the Mini Analysis program (Synaptosoft, Decatur, GA). Minis with a slow rise and falling time arising from neighboring electrically coupled muscle cells were excluded from analysis (Gho, 1994; Zhang et al., 1998). Data are reported as mean ± SEM, unless otherwise specified. A one-way analysis of variance followed by Tukey's Honest Significant Difference test was used to assess statistically significant differences among the genotypes. Differences were considered significant at $P < 0.05$.

2.11. Physical interaction between MTGO and CCT3

2.11.1. Plasmids for production of GST fusion proteins

The vector used for generating GST fusion proteins was pGEX-LB, a derivative of pGEX-4T-1 (Amersham-Pharmacia Biotech). In pGEX-LB, a "rigid" Pro residue is replaced with a "flexible" Gly-Gly-Gly-Gly-Ser-Gly coding sequence to promote the independent functioning of the GST and fusion moieties (Bardwell et al., 2009). Plasmid pGEX-dmCCTγ (for expressing *Drosophila* CCT3) was constructed as follows. A full-length cDNA encoding *Drosophila* CCT3 (FBgn0015019, GenBank AY089543.1) was obtained from the Drosophila Genomics Resource Center (DGRC, Bloomington, IN), clone LD20933, stock number 3646. The 2.0 kb cDNA insert is cloned in pBS (SK-) with the T3 promoter proximal to the 5' end of the cDNA. The cDNA insert was verified by Sanger sequencing. This plasmid (designated pBS_SK(-) RevComp_Dros_Cct_gamma) was used as the template in a site-directed mutagenesis reaction with primers JB-cctγ-*Bam*HI-s, JB-cctγ-*Bam*HI-as, JB-cctγ-*Sal*I-s, and JB-cctγ-*Sal*I-as to generate plasmid pBSSK-dmCCTγ-*Bam*HI-*Sal*I (see Supplemental Table 3 for primer sequences). This procedure inserted a *BamH*I site in the appropriate frame upstream of the CCT3 open reading frame and a *Sal*I site distal to the termination codon. This *BamH*I and *Sal*I fragment was excised and inserted into pGEX-LB that had been cut with the same enzymes, yielding pGEX-dmCCTγ. The G297D mutant was generated from pGEX-dmCCTγ by site-directed mutagenesis using primers JB-cctγ-G297D-s and JB-cctγ-G297D-as. QuikChange and QuikChange-Multi kits (Agilent Technologies, Santa Clara, CA) were used for all site-directed mutagenesis reactions. All changes were confirmed by DNA sequencing.

2.11.2. Plasmids for production of in vitro transcribed and translated MTGO and derivatives

A full-length cDNA encoding *Drosophila CG42389-RF (mtgo-RF)* (GenBank BT133431.1) was obtained from the DGRC (clone FI20237, stock number 1645047). The 6.4 kb cDNA insert is cloned in pFLCI, a modified pBluescript (SK+) vector, with the T7 promoter proximal to the 5' end of the cDNA. The cDNA insert was verified by sequencing. To allow efficient transcription of *mtgo-RF* using T7 RNA polymerase, the 842 bp 5′ UTR of *mtgo-RF* was removed by digestion with *Not*I and *Nco*I, then blunt ended using T4 DNA polymerase followed by ligation to produce pFLCI mtgo-RF-D5UTR, which is hereafter referred to as pT7-MTGO(1–1762). The amino-acid sequence for MTGO(1–1762) is shown in Supplemental Fig. 1 (CG42389-PF).

The MTGO truncations MTGO(1–626) and MTGO(1–1020) were derived from pT7-MTGO(1–1762) by introducing stop codons at codons 627 and 1021 of the MTGO coding sequence via site-directed mutagenesis. The sense primers for these mutagenesis reactions were JB-mtgoI627TAAstop-s and JB-mtgoP1021TAAstop-s, respectively (Supplemental Table 3). Plasmid pT7-MTGO(620–1762), encoding the N-terminal deletion MTGO(620–1762), was derived from pT7-MTGO(1–1762) in two steps, and took advantage of the fact that pT7-MTGO(1–1762) contains only a single *Nco*I site, which overlaps with the initiation codon of MTGO. First, site-directed mutagenesis was used to insert a second *Nco*I site in the appropriate reading frame in front of codon 620, using primers JB-mtgo-*Nco*I-620-s and JB-mtgo-*Nco*I-620-as. Next, the fragment containing codons 2–619 was excised by digestion with *Nco I* and the remainder of the plasmid was recircularized, reforming a single *Nco I* site. The first five amino acids of the encoded protein are MENSI, where the E corresponds to residue 620 in the full-length protein. The plasmid encoding MTGO(474–1762) was constructed by a similar procedure, using primers JB-mtgo-*Nco*I-474-s and JB-mtgo-*Nco*I-474-as. The first five residues of this protein are MAPQP, where the first proline corresponds to residue 474 in the full-length protein. The plasmid encoding MTGO(1021–1762) was also constructed by a similar procedure, using primers JB-mtgo-*Nco*I-1021-s and JB-mtgo-*Nco*I-1021-as. The first five residues of this protein are MAPHC, where the first proline corresponds to residue 1021 in the full-length protein.

Plasmids encoding MTGO(1–1738) and MTGO(620–1738) were derived from pT7-MTGO(1–1762) and pT7-MTGO(620–1762) respec-

tively, by introducing a stop codon at codon 1739 of the MTGO coding sequence by site-directed mutagenesis using primers JB-mtgo-A1739TAAstop-s and JB-mtgo-A1739TAAstop-as. Likewise, the plasmids encoding MTGO(1–1560), MTGO(620–1560) and MTGO(1021–1560) were derived from pT7-MTGO(1–1762) and pT7-MTGO(620–1762) respectively, by introducing a stop codon at codon 1561 of the MTGO coding sequence by site-directed mutagenesis using primers JB-mtgo-S1561TAAstop-s and JB-mtgo-S1561TAAstop-as. Supplemental Table 3 contains information on all primer sequences used to construct the MTGO and *Dmel* CCT3 expression vectors. All MTGO derivatives were confirmed by DNA sequencing.

2.11.3. Protein purification

GST fusion proteins were expressed in bacteria, purified by affinity chromatography using glutathione-Sepharose (GE Healthcare, Chicago, IL) and quantified as described (Bardwell et al., 2009; Bardwell et al., 2001; Whisenant et al., 2010).

2.11.4. In vitro transcription and translation

Proteins labeled with [^{35}S]-methionine were produced by coupled transcription and translation reactions (T7, Promega Corporation, Madison, WI). Translation products were partially purified by ammonium sulfate precipitation (Bardwell and Shah, 2006), and resuspended in binding buffer (20 mM Tris-HCl (pH 7.5), 125 mM KOAc, 0.5 mM EDTA, 1 mM DTT, 0.1% (v/v) Tween-20, 12.5% (v/v) glycerol) prior to use in binding assays. In addition to the complete translation product, multiple faster-migrating forms of lower molecular mass were observed, in particular with the full-length MTGO. Such faster-migrating forms are often seen in cell-free translation reactions and are typically caused by a low frequency of premature translation termination or internal initiation (Struhl, 1991). *Mtgo-RF* encodes a 1762 residue protein with a calculated molecular mass of 190 kDa, although full-length MTGO migrated with an apparent molecular mass of 250 kDa on a 10% SDS-PAGE gel. This is consistent with other studies in which proline-rich proteins migrate more slowly than their calculated molecular weight (Lane and Crawford, 1979; Linzer and Levine, 1979).

2.11.5. Protein binding assays and protein gel electrophoresis

Protein binding assays were performed as described (Bardwell et al., 2001; Gordon et al., 2013). Briefly, ^{35}S-radiolabeled full-length MTGO protein and shorter derivatives thereof were prepared by in vitro translation and ~1 pmol of each derivative was incubated with 25 μg of GST or GST-CCT3 bound to glutathione-Sepharose beads. Bead-bound complexes were collected by sedimentation, washed extensively, and then analyzed by 10% SDS-PAGE. A sample of each MTGO derivative corresponding to 2% of the amount added in the binding reactions was loaded into lanes marked 'Input'. SDS-PAGE gels were analyzed by staining with GelCode Blue (Thermo Scientific) for visualization of the bound GST fusion protein and by exposure to a phospho-storage screen for visualization of the bound radiolabeled protein. Quantification of binding was performed with a Typhoon TRIO + Imager (GE Healthcare) using phosphorimaging mode. Percent binding was determined by comparing the input with the amount that was co-sedimented. Each binding assay was repeated in a minimum of three independent experiments; i.e. experiments performed on different days, with fresh preparation of GST-fusion proteins and in-vitro translated proteins. Technical replicates (two per experiment) were averaged to obtain a single data point.

2.11.6. Statistical analysis

Statistical analysis of binding assay results was performed using Welch's unequal variance *t*-test with two tails (Ruxton, 2006). This was accomplished in Microsoft Excel using the T.TEST function, setting the 'tail' option to 2, and the 'type' option to 3.

3. Results

3.1. Drosophila CG42389 is an essential gene that encodes orthologs of vertebrate FNDC3 proteins

A scan of proteins encoded by the *Drosophila* genome identified *CG42389,* which we named *miles to go* (*mtgo),* as the only locus capable of encoding FNDC3 orthologs in *D. melanogaster* (Supplementary Table 1). As described later, the mutant was named due to the phenotype where wandering larva move without pauses or head-sweeps during olfactory testing, ('Miles to go before I sweep' (*sic*)), combined with the incomplete branching and elongation of the larval NMJ. Alignment of cDNAs with genomic sequence, plus RNA-seq data (FlyBase.org), suggests *mtgo* is transcribed from three independent promoters producing *-RE*, *-RF* and *-RG* transcripts (Fig. 1). Each transcript produces a protein with a different amino-terminal sequence (-PE, -PF and –PG; Supplementary Fig. 1), although all three proteins contain a proline rich N-terminus (Supplementary Table 2) and contain the same nine FN3 domains and tail-anchoring (TA) sequence (Supplementary Fig. 1). All of the FN3 domains in *mtgo* are encoded by a single exon. In contrast, the FN3 domains in orthologous *Fndc3* genes in mammals and other chordates are distributed over multiple exons (Fig. 1). To investigate the function of *mtgo* in development we analyzed ten uncharacterized insertion alleles of *mtgo* available from the Bloomington stock center (Fig. 1 and Materials and Methods). Two alleles ($mtgo^{e02963}$ and *Mi{MIC}* $mtgo^{MI11367}$) were lethal as homozygotes and as *trans* heterozygotes, which suggests that the mutant phenotypes result from allelic insertions. The other alleles showed no phenotype and were not studied further.

Based on the insertion site of the PBac in the $mtgo^{e02963}$ allele we predicted the *–RF* isoform would be predominantly affected. Indeed, quantitative RT-PCR of the *-RE* and *-RF* transcripts in wild type and mutant animals showed that the *-RF* transcript is reduced to ~23% in $mtgo^{e02963}$ heterozygotes, and to ~0.01% in $mtgo^{e02963}$ homozygote animals (Materials and Methods). In contrast, the longer *-RE* transcript which contains the $mtgo^{e02963}$ PBac insertion in the middle of a 92.8 kb intron was only mildly affected (~64% of WT in homozygotes) and the quantity of *-RG* transcripts was similar between adult wild-type and heterozygous and homozygous mutant $mtgo^{e02963}$ flies. Hence, the $mtgo^{e02963}$ allele results in loss of the *-RF*, but not the *-RE* and *-RG* transcripts from the *mtgo* locus.

3.2. Mtgo mutant animals exhibit late pupal lethality, ataxia and reduced lifespan

To identify the lethal phase of $mtgo^{e02963}$ and $mtgo^{MI11367}$ mutants, we scored the number of heterozygous and homozygous animals at early (L1) and late (L3) larval, pupal and adult stages. No difference was observed in numbers of heterozygous and homozygous $mtgo^{e02963}$ animals at L1 (χ^2 = 2.03, 1 *df*, P = 0.1542) or L3 (χ^2 = 0.28, 1 *df*, P = 0.5938). However, only ~3% of the expected number of $mtgo^{e02963}$ homozygotes eclosed as adults when reared at 25 °C (χ^2 = 214.25, 1 *df*, P < 0.0001). Abdominal peristalsis and weak pumping of the ptilinum was observed in late stage (dark) homozygous $mtgo^{e02963}$ pharate adults indicating the animals were viable at this stage. When manually removed from the puparium, homozygotes were able to inflate their wings and walk although they displayed an ataxic gait. Such rescued, and rare self-eclosed homozygote $mtgo^{e02963}$ adult flies had shorter life-spans (males 13.2 ± 6.0 days (n = 29); females 9.5 ± 7.2 days (n = 21)). For comparison, the median lifespan of wild-type control Canton-S *Drosophila* maintained under the same conditions is ~59 days (Pallos et al., 2008). Animals homozygous for the $mtgo^{MI11367}$ allele that eliminates all three transcriptional isoforms exhibited the same late-pupal-lethal phase as animals homozygous for the $mtgo^{e02963}$ allele. Almost all heteroallelic heterozygote $mtgo^{e02963/MI11367}$ animals also

died at late-pupal phase (Materials and Methods) with death often occurring during eclosion. Hence, *mtgo-RF* is required for pharate animals to exit the pupal case, the overt phenotypic consequences of loss of all three isoforms appear no more severe than loss of the *-RF* isoform alone, and rare escaper *mtgo*-mutant adults have reduced lifespan.

3.3. Mtgo is expressed in the CNS and ventral nerve cord in wandering stage larvae

The defect in pharate eclosion and ataxia observed in rare adult homozygous $mtgo^{e02963}$ escapers suggested that *mtgo* might be required for nervous system development or function. To investigate whether *mtgo* is expressed in the larval nervous system, we used flies homozygous for the $mtgo^{CPTI001586}$ allele (hereafter referred to as $mtgo^{EYFP}$) in which a RNA splice acceptor (SA) - EYFP (mVenus) coding sequence - RNA splice donor (SD) "protein-trap" cassette is inserted within intron 3 of the *-RF* transcript (Fig. 1) (Lowe et al., 2014). We verified the insertion caused an in-frame fusion of the EYFP coding sequence within the proline rich region (PRR) encoded by *mtgo-RE* and *mtgo-RF* by reverse transcriptase (RT)-PCR and DNA sequencing using RNA isolated from homozygous $mtgo^{EYFP}$ larvae and adult animals (Supplementary Fig. 3). We were unable to determine the cellular expression pattern of the *mtgo-RG* isoform because the EYFP protein trap does not affect this isoform and because the exons unique to the *mtgo-RG* isoform are too short and expressed at too low a level to be uniquely detected by in situ hybridization. The significant reduction in levels of the wild-type -RF mRNA isoform in the viable homozygous $mtgo^{EYFP}$ animals (Supplementary Fig. 3) suggests the MTGO-EYFP fusion proteins retain at least some MTGO function.

To identify where MTGO-EYFP is expressed in larvae, homozygous $mtgo^{EYFP}$ and negative-control Canton S wandering larvae were dissected and examined using DIC/Nomarski and fluorescence confocal microscopy. No background fluorescence was observed in wild-type Canton S larval nervous system (Supplemental Fig. 4D, E). In homozygous $mtgo^{EYFP}$ wandering larvae, very low-level EYFP fluorescence was found predominantly in the CNS (Fig. 2A, Supplemental Fig. 4B) and ventral nerve cord (VNC) (Fig. 2A,B) with relatively weak signal in the body wall muscles (Supplemental Fig. 4F,H). In the CNS, MTGO-EYFP localized predominantly to neuropil glial cells (Fig. 2A, Supplemental Fig. 4B), while in the VNC the fluorescence was present at low levels within neurons in general (Fig. 2A), including some whose location and morphology appear consistent with peptidergic (Park et al., 2008) and motor neurons (Kim et al., 2009; Sink and Whitington, 1991). Due to the extremely low-level EYFP signal we were unable to confirm these cell identities using co-expression of Gal4 > RFP driver lines whose relatively high level of RFP expression confounded use of photon counting to detect the EYFP signal. Development of an anti-MTGO antisera is required to verify the identity of the neurons expressing MTGO. MTGO-EYFP localized in a punctate manner within the cytoplasm of the cell bodies of the presumptive motoneurons (Fig. 2B) and was also observed in axons emerging from the VNC ganglia (Fig. 2B) and axons from motoneurons in proximity to muscles (Supplemental Fig. 4F-H). The MTGO-EYFP signal in axons often appeared more intense at the periphery of the axon (Supplemental Fig. 4F,H). Relatively weak EYFP signal at the limit of detection using photon counting mode was observed in the muscle (Supplemental Fig. 4F,H). No EYFP signal was observed in trachea (Supplemental Fig. 4F-H). Hence, EYFP-MTGO is expressed in both neurons and glia in the larval nervous system, and at lower levels in body wall muscles which supports a potential requirement for MTGO in these cell types during development.

3.4. Mtgo mutants have abnormal terminal axonal arborization of the NMJ

The failure of $mtgo^{e02963}$ homozygote larvae to eclose could be due to many different reasons including defects in neuronal or muscle function. To determine if the larval neuromuscular junction (NMJ) formed normally, we examined the structure of the NMJ in muscles 6 and 7 (6/7) in wild-type and homozygous mutant $mtgo^{e02963}$ wandering third-instar larvae. Filleted larvae were fixed and stained with anti-horseradish peroxidase (HRP) antisera (stains neuronal membranes), and anti-Discs Large (DLG) antisera (stains the post-synaptic muscle membrane surrounding Type Ib and Type Is boutons in NMJs) (Lahey et al., 1994; Packard et al., 2002). Examination of muscles 6/7 in

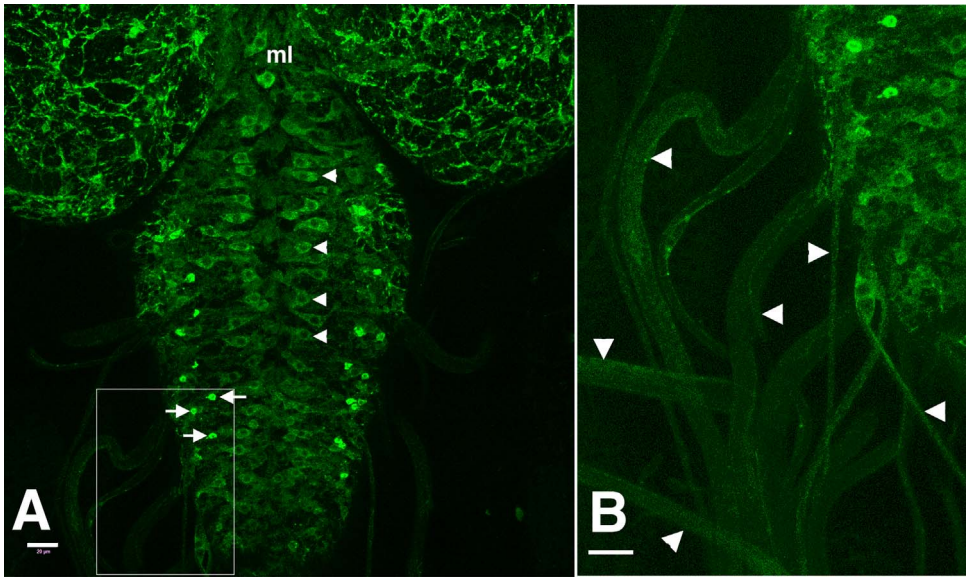

Fig. 2. Expression of MTGO-EYFP in nervous system of homozygous $mtgo^{EYFP}$ wandering third-instar larvae. (A,B) - Dissected CNS and ventral nerve cord (VNC) from homozygous $mtgo^{EYFP}$ late larva imaged for EYFP fluorescence (green). (A) In the nervous system in $mtgo^{EYFP}$ animals, EYFP is localized to the CNS in a neuropil glial pattern with neuronal localization in the VNC. Punctate cytoplasmic fluorescence is observed in the bodies of cells whose identity is consistent with motoneurons (e.g. arrowheads). Several cells lateral to these have relatively intense fluorescence (short arrows) whose distribution and pattern is similar to DIMM-positive neurons (Park et al., 2008). (B) Higher magnification of the boxed area in panel A showing fluorescence localized to axons (arrowheads) emerging from VNC ganglia. No fluorescence was observed in trachea, nor in negative control Canton S wandering third-instar larvae (Supplemental Fig. 4). ml – VNC midline. Scale bars (A) - 20 μm; (B) - 15 μm.

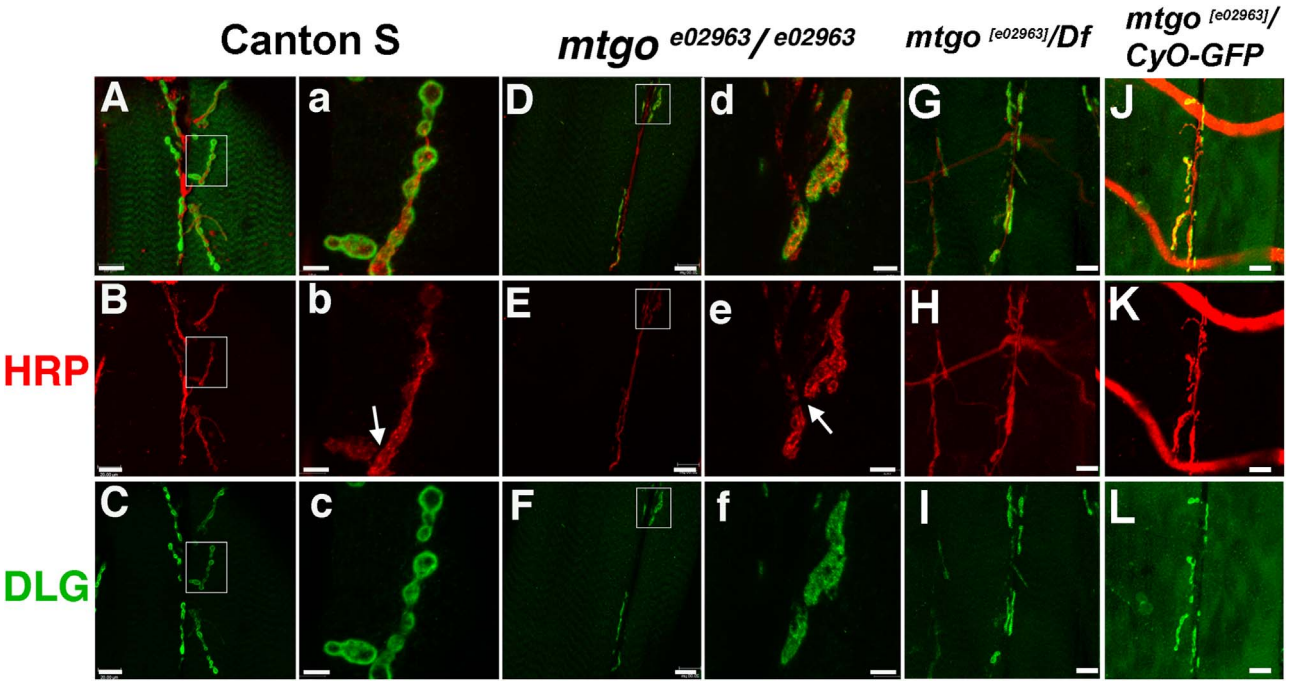

Fig. 3. Abnormal NMJ in muscles 6 and 7 in *mtgo*^{e02963} homozygote third instar larvae. Morphology of NMJ in abdominal body wall muscles 6/7 in segment A2 in (A-C) third instar wild-type Canton S, (D-F) homozygous *mtgo*^{e02963}, (G-I) *mtgo*^{e02963} */Df* and (J-L) *mtgo*^{e02963} */CyO-GFP* larvae. Maximum projections of Z-series confocal images. Areas boxed in white are shown at higher magnification in the right adjacent panel with lowercase letter. (A,a) Wild-type Canton S larvae showing normal pattern of synaptic boutons in NMJ. Anti-HRP ((B) neuronal membrane, red) and anti-DLG ((C) post-synaptic muscle, green) are shown in separate channels. (D-F) NMJ in homozygous *mtgo*^{e02963} larvae. Examples of branches are denoted by the white arrows in panels (b) and (e). Note the reduction in branching of the motor neuron terminus in panel (D). A five-fold increase in laser power was used to illuminate DLG-specific secondary antibody in panel F compared to panel C. Almost no DLG staining is observed in panel F when same laser power and detector gain is used as in panel C. Samples were prepared in parallel. (G-L) NMJ 6/7 from *mtgo*^{e02963} */Df* have similar appearance to *mtgo*^{e02963} homozygotes, while heterozygous *mtgo*^{e02963} have an appearance intermediate to that of Canton S and *mtgo*$^{e02963/\ e02963}$. Scale bars – 20 μm (panels with uppercase letters); 5 μm (panels with lowercase letters).

abdominal segment 2 (A2) revealed abnormal NMJ morphology in *mtgo*^{e02963} homozygotes (Fig. 3). Although motoneuron axonal pathfinding to target muscles appeared normal, branching of the motoneuron terminus was severely reduced and was restricted to the margin between muscles 6/7 (Fig. 3D,G). In *mtgo*^{e02963} homozygotes the DLG-based morphology of the post-synaptic membrane also appeared less discrete (Fig. 3f) compared to the rounded individual boutons in wild-type animals (Fig. 3c). Heterozygous mutant *mtgo*^{e02963} animals displayed an intermediate phenotype (Fig. 3J-L) suggesting a dose-dependent requirement of MTGO for normal NMJ development.

To better define the abnormal NMJ development in *mtgo* mutants, we quantified the number and length of branches and number of boutons for the NMJ at muscle 6/7 (Fig. 4A). *Mtgo*^{e02963} homozygotes had fewer and shorter branches as well as fewer boutons. Heterozygote *mtgo*^{e02963} larvae had an intermediate reduction in number of boutons, branches and branch length, suggesting that dosage of *mtgo* function is important for normal NMJ development. No difference was observed in the combined size of muscles 6 and 7 between the three genotypes (WT = 46,893 ± 5883 μm^2, n = 5; HET = 45,222 ± 6899 μm^2, n = 3; HO = 51,384 ± 2397 μm^2, n = 3. Values = mean, ± SE. p = 0.787, one-way ANOVA with Tukey's *post-hoc* test). Homozygous and heterozygous *mtgo*^{MI11367} larvae showed disruptions of the NMJ similar to those observed in *mtgo*^{02963} homo- and heterozygotes, suggesting that loss of all three isoforms of *mtgo* does not enhance the NMJ phenotype compared to loss of the *-RF* isoform alone. *Mtgo*^{e02963} hetero- and homozygous larvae also had a dramatic increase in ghost boutons per NMJ (Fig. 4A,B). The formation and maintenance of synaptic structures requires both anterograde signaling from the neuron to the muscle and retrograde signaling from the muscle to the neuron (Menon et al., 2013). Ghost boutons (Ataman et al., 2006) are transitional structures that have not yet formed mature boutons and are not derived from degeneration of mature boutons (Menon et al., 2013). They display the pre-synaptic marker HRP but have no apposing post-synaptic structure (Ataman et al., 2006). Such boutons can form due to defects in anterograde signaling (e.g. wingless (WG) signaling) between the neuron and the post-synaptic muscle (Ataman et al., 2006).

Microtubule organization is important for normal NMJ formation and homeostasis (Prokop et al., 2013) and branching of the NMJ nerve terminus correlates with conversion of a microtubule loop-like structure within a bouton into a “fan-like” or splayed structure that resolves to form two branches that subsequently elongate, with new loops forming within boutons periodically along the branches (Roos et al., 2000; Zito et al., 1999). *Futsch* encodes a MAP1B-like microtubule-associated protein required for this process (Hummel et al., 2000; Roos et al., 2000). To determine if *mtgo* mutant larvae were unable to form either microtubule ‘loops’ or ‘splays’, we examined the morphology of Futsch staining. No obvious difference was observed in the gross morphology of these structures in NMJs in *mtgo*^{e02963} homozygotes and Futsch staining was located throughout the nerve ending (Supplemental Fig. 5). However, quantitative differences in the ability of these subcellular structures to progress to distinct synaptic branches would not have been detectable in our analysis.

In summary, the data indicate that *mtgo-RF* is required for normal formation and branching of the axon terminal and formation of boutons, and reduction or absence of *mtgo-RF* results in the presence of ghost boutons. The data also suggest that *mtgo-RF* is required in a dose-dependent manner for normal NMJ development. Additional studies are required to verify the predicted dose-dependent effect and to understand its mechanism.

3.5. Expression of mtgo-RF in neurons, but not muscle, rescues lethality and NMJ phenotypes in *mtgo*^{e02963} and *mtgo*^{MI11367} homozygotes

Analysis of *mtgo*^{EYFP} larvae showed that MTGO is expressed in the CNS and at lower levels in muscle during larval development (Fig. 2).

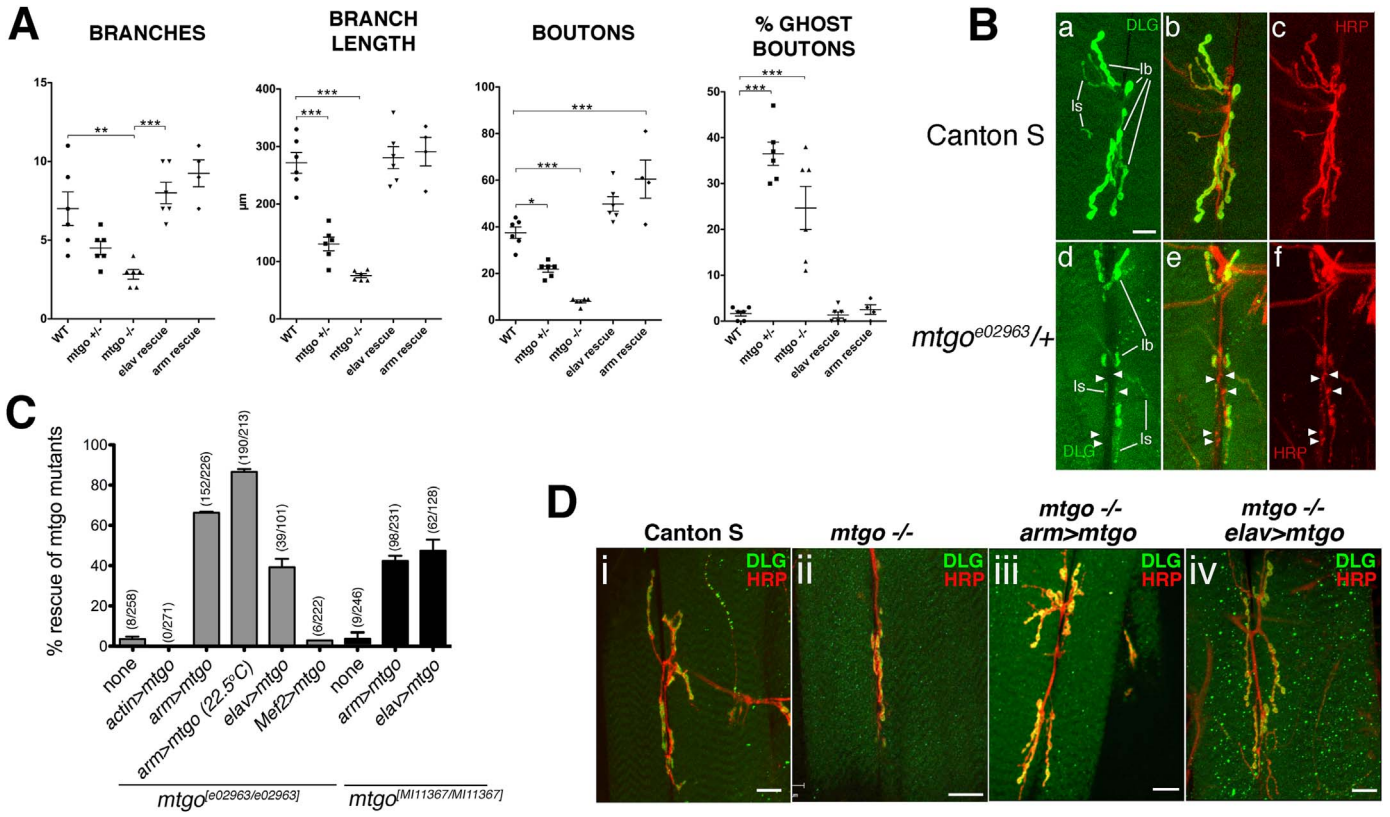

Fig. 4. Quantitative analysis of defects in muscle 6/7 NMJ in *mtgo*^{e02963} larvae and rescue of NMJ phenotype and lethality by expression of *mtgo-RF* in neurons, but not muscle. (**A**) Quantification of branches, length of branches, boutons and ghost boutons per muscle 6/7 NMJ in wildtype, heterozygous and homozygous *mtgo*^{e02963} larvae, plus homozygous mutant larvae expressing *mtgo-RF* in neurons (*elav* rescue) or all tissues (*arm* rescue). Symbols represent individual data points. Mean and standard error are shown for each data set. N = 6 independent biological replicates for all groups except *arm* rescue (n = 4). Significance values of < 0.05, < 0.01 or < 0.001 between categories are denoted by one, two or three asterisks, respectively. (**B**) Example of ghost boutons (white arrowheads) in muscle 6/7 NMJ from *mtgo*^{e02963}*/CyO-GFP* L3 larva (d-f). Ghost boutons were not observed in wild-type Canton S animals (a-c). DLG - discs large staining (post-synaptic SSR); HRP - horseradish peroxidase (neurons). Ib and Is denote type Ib and type Is boutons respectively. (**C**) Viability of *mtgo*^{e02963} (*RF*-transcript null) or *mtgo*^{MI11367} (all transcript null) homozygote flies, including mutants containing the *UAS > mtgo-RF* transgene in combination with different *Gal4* drivers. Data are expressed as percentage of recovered versus expected *mtgo*^{e02963} homozygote (RF) or *mtgo*^{MI11367} (null) homozygote, *UAS-mtgo-RF;* GAL4 animals. The number of (recovered/expected) *mtgo* mutant flies is shown in parentheses above each bar. All experiments were conducted at 25 °C except as shown. Partial rescue of *mtgo*^{e02963} or *mtgo*^{MI11367} pharate lethality by expression of *mtgo-RF* by *arm > Gal4* and *elav > Gal4,* but not *Mef2 > Gal4,* was observed. No *actin > Gal4*; *UAS-mtgo-RF* animals could be recovered on either a wild-type or *mtgo*^{e02963} homozygous background, indicating lethality due to over-expression of *mtgo-RF* driven by the *actin* > Gal4 driver. Due to failure to rescue the mutant phenotype with two different muscle-specific (*Mef2* and *c179*) *Gal4* drivers, these experiments were not repeated in the *mtgo*^{MI11367} mutant background. (**D**) Phenotype of muscle 6/7 NMJ in wandering third-instar larvae from (i) wild-type; (ii) *mtgo*^{e02963} homozygote; (iii) *mtgo*^{e02963} homozygote with *UAS-mtgo-RF* and *arm > Gal4* driver and (iv) *mtgo*^{e02963} homozygote with *UAS-mtgo-RF* and *elav > Gal4* driver. The green (DLG) puncta observed in mutants is non-specific staining that can also be detected in other samples at a lower level. Scale bar is 20 µm for all panels in (B) and 24 µm in each panel in (D).

These results were independently supported by analysis of expression of *mtgo* in various databases (flyatlas.org, flymine.org, flybase.org) and a study of gene expression during differentiation of *Drosophila* neuroblasts into neurons (Berger et al., 2012). To determine the tissue specific requirements of *mtgo* during development, transgenic flies carrying a *UAS-mtgo-RF* cDNA construct were tested for their ability to rescue animals homozygous for the RF-isoform-deficient (*mtgo*^{e02963}) or the pan-isoform-null *mtgo* (*mtgo*^{MI11367}) alleles when expressed in different tissues.

We quantified the ability of *actin* > Gal4 (high level expression in all tissues), *arm > Gal4* (low-level expression in all tissues), *elav > Gal4* (expression in all neurons and transiently in embryonic glia) and *Mef2 > Gal4* (expression in muscle) drivers to rescue both alleles by expressing *UAS > mtgo-RF*. Expression of *mtgo-RF* driven by the *arm > Gal4* driver rescued both *mtgo* mutations, with ~90% rescue when flies were propagated at 22.5 °C compared to ~70% rescue at 25 °C (Fig. 4C). Because gene expression from the Gal4 drivers at 22.5 °C is approximately half that at 25 °C (Song et al., 2013), the enhanced rescue at lower temperature suggests an optimum level of *mtgo* gene expression is important for normal development. Consistent with this notion, expression of *mtgo-RF* driven by a relatively strong *actin > GAL4* driver caused lethality (Fig. 4C). Expression in muscles driven by the *Mef2 > Gal4* driver (Ranganayakulu et al., 1996) (Fig. 4C) was unable to rescue *mtgo*^{e02963} homozygotes. By contrast, crosses using an *elav > Gal4* (neuronal) driver provided ~40% rescue of the pharate lethality in both *mtgo*^{e02963} and *mtgo*^{MI11367} homozygotes (Fig. 4C). An increased number of boutons was observed in the *arm > Gal4* rescued larvae compared to wildtype Canton S larvae (Fig. 4A,D), also supporting a dose-dependent function of MTGO in NMJ development. Morphology of type Ib and type Is boutons appeared grossly normal in homozygote *mtgo*^{e02963} flies rescued using the *arm > Gal4* and *elav > Gal4* drivers (Fig. 4D) in combination with the *UAS > mtgo-RF* transgene.

The normal DLG staining observed in the post-synaptic muscle surrounding boutons in *Elav > Gal4* rescued animals suggests MTGO activity in neurons has a cell-extrinsic effect on DLG expression and organization in the post-synaptic side of the NMJ. In turn, this suggests the large increase in ghost boutons in *mtgo* mutant larvae is caused by abnormal signaling from the nerve, rather than inability of the post-synaptic muscle to sense or respond to signals from the neuron. Thus, *mtgo-RF* is required in a dose-dependent manner for NMJ development, expression of *mtgo-RF* in the neuron but not the post-synaptic muscle is sufficient to rescue the NMJ mutant phenotype, over-expression of *mtgo-RF* causes lethality, and the *mtgo-RF* isoform is

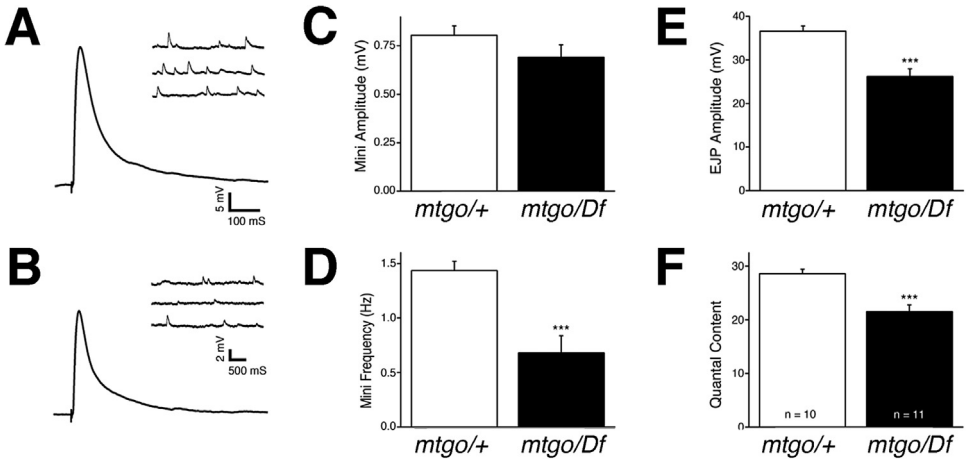

Fig. 5. Defective neurotransmission at NMJ in *mtgo*^{e02963} wandering third-instar larvae.(A,B) - Representative traces of evoked excitatory junctional potentials (EJPs) from NMJ of (A) heterozygote *mtgo*^{e02963} (*mtgo/+*) and (B) trans-heterozygote *mtgo*^{e02963}/*Df* mutant larvae. A ~30% reduction in EJPs is observed in homozygote mutant larvae compared to heterozygotes. C-F – Quantification of reduction in (C) amplitude, (D) frequency of spontaneous mini's, (E) evoked EJP amplitude and (F) quantal content of trans-heterozygote *mtgo*^{e02963}/*Df* (*mtgo/Df*) larvae compared to *mtgo*^{e02963} (*mtgo/+*) heterozygotes. Number of animals analyzed = 10 for heterozygote *mtgo*^{e02963} and 11 for trans-heterozygote *mtgo*^{e02963}/*Df* mutant. *** p = < 0.001.

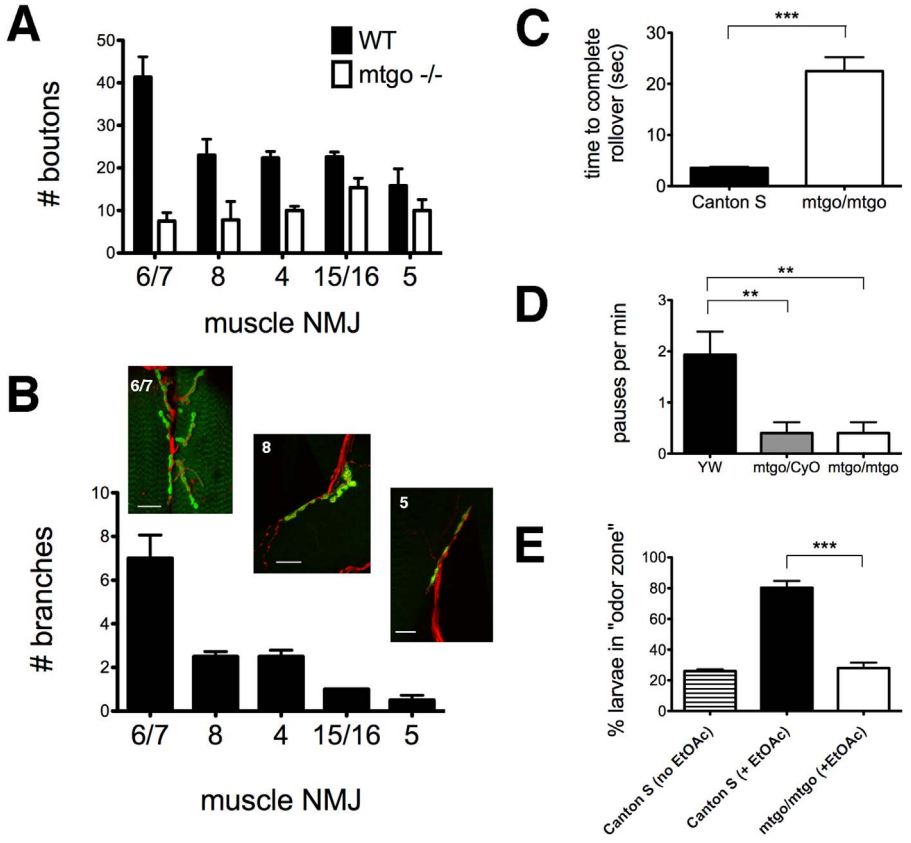

Fig. 6. Mutation of *mtgo* preferentially affects development of branched *vs* unbranched NMJ and alters righting-behavior, olfaction and pausing in *mtgo*^{e02963} wandering third-instar larvae. (**A**) Number of boutons in muscles 6/7, 8, 4, 15/16 and 5 in segment A2 in WT (Canton S) or *mtgo*^{e02963} homozygous mutant L3 wandering-larvae. N = 6 independent animals for each genotype except muscle 4 where n = 3. Values are mean ± SEM. P values for each set of muscles are P < 0.0001 for muscles 6/7; P = 0.0003 for muscle 4; P = 0.0005 for muscle 8; P = 0.0002 for muscles 15/16 and P = 0.02 for muscle 5. (**B**) Number of branches per NMJ in muscles 6/7, 8, 4, 15/16 and 5 in WT animals. N = 6 independent animals, except muscle 4 where N = 3. Values are mean ± SEM (error bar is small but present for muscle 15/16). Images show example of representative NMJ's for muscles 6/7, 8 and 5 (Scale bars = 25 µm for muscle 6/7, 20 µm for muscle 8; and 18 µm for muscle 5).(**C**) Self-righting (rollover) behavioral assay. Time to complete rollover for *mtgo*^{e02963} homozygote and control Canton S L3 wandering larvae. ***= P < 0.001.(**D**) Number of 'pauses' (i.e. rearing and head sweeps) per min during the five-min test period for 15 independent *mtgo*^{e02963} homozygote and control YW animals. ** = P < 0.01. (**E**) Proportion of Canton S or *mtgo*^{e02963} homozygote larvae within odor zones two min after 50 larvae were placed in center of each petri dish. ***= P < 0.001.

both necessary and sufficient to complement *mtgo* null mutations that affect all three transcripts.

3.6. *Mtgo*^{e02963} mutant larvae display abnormal NMJ synaptic electrophysiology

The presence of ghosts in *mtgo* mutants and a requirement for *mtgo* on the pre-synaptic side of the NMJ are both consistent with a pre-synaptic deficit in *mtgo* mutants. As an independent method to test this prediction we performed electrophysiology on NMJ's in heterozygous *mtgo*^{e02963} and *mtgo*^{e02963}/Df(2L)ED1109 larvae. Evoked excitatory junctional potentials (EJPs) generated in response to vesicular release of glutamate from the motoneuron, and spontaneous miniature end plate potentials ("mini's"; i.e. the amplitude of the response to a single vesicle release, also known as quantal size) were recorded from the NMJ of muscle 6/7 in third-instar larvae (Fig. 5 A,B). Although amplitude of miniature potentials was not significantly different (Fig. 5C), their frequency was reduced by ~60% in *mtgo*^{e02963}/*Df(2L)* ED1109 larvae (Fig. 5D). In addition, the average EJP amplitude in third-instar *mtgo*^{e02963}/Df(2L)ED1109 larvae was ~30% reduced compared to heterozygous animals (*mtgo*^{e02963}/+ = 37 mV ± 1 mV; n = 10; *mtgo*^{e02963}/*Df(2L)*ED1109 = 27 mV ± 2 mV; n = 11) (Fig. 5E). Quantal content (i.e. the number of vesicles released per evoked event) was also reduced in *mtgo*^{e02963}/*Df(2L)*ED1109 compared to *mtgo*^{e02963}/+ larvae (Fig. 5F). Together with the reduced branching and reduced number of boutons observed in *mtgo*^{e02963} larvae, these results suggest NMJs in *mtgo* mutants have a smaller number of active zones that can function in a grossly normal manner. Hence, *mtgo*-RF is required for normal formation and function of the larval NMJ, and loss of function of *mtgo-RF* produced reduced elaboration and decreased synaptic activity of the motoneuron endplate.

3.7. Mutation of mtgo disproportionally affects bouton number in normally highly branched vs less branched NMJs

Mtgo mutant larvae show a striking reduction in terminal arborization of the muscle 6/7 NMJ. In wild-type animals this NMJ is relatively highly branched with the two adjacent muscles being innervated by the same motoneuron (Atwood et al., 1993; Hoang and Chiba, 2001; Ruiz-Canada and Budnik, 2006). We investigated whether *mtgo* homozygous mutant larvae had fewer boutons in NMJ's that are normally less branched. To do so, we compared the number of boutons in muscles that are highly branched (muscles 6/7), moderately branched (muscles 8, 4) or few, or unbranched (muscles 15/16 and 5) NMJ's in homozygous *mtgo*^{e02963} and wild-type control animals (Fig. 6A). The results showed a disproportionally greater reduction in bouton number in highly branched neurons (only 18% of boutons remaining compared to control in muscles 6/7) compared to unbranched neurons (70% of boutons remain compared to control in neurons innervating muscles 15/16 or 5; Fig. 6A). This suggests that the reduced number of boutons in *mtgo*^{e02963} mutant larvae is at least partly a consequence of a reduced ability of NMJ's to branch.

3.8. *Mtgo*^{e02963} larvae exhibit abnormal behavior consistent with altered neurological function

Because *mtgo-RF* function is required in neurons during development and is expressed in the CNS, we screened for evidence of behavioral changes in homozygous *mtgo*^{e02963} wandering larvae that might result from abnormal neuronal function. A rollover assay was performed to test proprioception and ability to self-right, a complex behavior requiring motor control (Bodily et al., 2001). L3 larvae were rolled on to their dorsum, and the time to complete righting was recorded (Fig. 6C). *Mtgo*^{e02963} homozygotes (n = 5) took ~6x longer (13.7 ± 1.7 s) to initiate the rollover compared with wild-type control larvae (2.1 ± 0.17 s; n = 5). Similarly, *mtgo*^{e02963} homozygotes took ~6x longer (22.5 ± 2.7 s; n = 5) to complete the rollover compared with wild-type control larvae (3.6 ± 0.2 s; n = 5; Fig. 6C). Mutant larvae required an average of 2.9 ± 0.4 peristaltic waves of the larval musculature to right themselves compared with a single wave for control animals. To determine if the increased time required for self-righting was secondary to a more generalized defect such as reduced muscle strength or stamina, we performed simple locomotion assays. No difference was observed in the speed of crawling of wild-type, heterozygote, and homozygote *mtgo*^{e02963} wandering larvae, including distance migrated per peristaltic wave or number of peristaltic waves per min.

We also screened for deficits in olfaction and simple avoidance behavior. Wandering third-instar larvae demonstrate stereotypical olfactory behavior associated with searching for food where animals pause, rear and move their head laterally (termed a head 'sweep' or 'cast') before recommencing crawling (Gomez-Marin and Louis, 2012; Gomez-Marin et al., 2011). Chemotaxis was tested in wild-type and homozygous-mutant *mtgo*^{e02963} larvae using ethyl acetate as a robust attractant (Khurana and Siddiqi, 2013). During these assays both heterozygote and homozygote *mtgo*^{e02963} larvae displayed reduced pausing and head sweep behavior (Fig. 6D) suggestive of abnormal olfaction. At the end of each trial period, ~80% of wild-type wandering larvae had entered an odor zone (Fig. 6E). In contrast, only ~25% of homozygous *mtgo*^{e02963} larvae had entered an odor zone, similar to the number of wild-type Canton S animals that had entered the same area zone in negative-control petri dishes in which filter discs lacked ethyl acetate (Fig. 6E). Wild-type and mutant larvae displayed no difference in either their touch withdrawal response or in light avoidance. In summary, in homozygous mutant *mtgo*^{e02963} larvae, locomotion, light avoidance and mechanosensory withdrawal reflexes appear normal, but olfaction and rollover behaviors are disrupted. These results suggest that *mtgo* is required for discrete complex behaviors and that a lack of *mtgo* function in larvae does not affect all neuronal pathways equally.

3.9. MTGO binds directly to the chaperonin CCT3

The chaperonin CCT3 (also known as CCTγ) was co-precipitated with MTGO in a large-scale *Drosophila* protein interaction screen (Lowe et al., 2014). Group II chaperonins are a family of cytosolic chaperone proteins that form a large double-stacked ring structure that encloses a substrate-binding cavity, with each ring composed of eight different, but related, proteins named CCT1 - 8 (Leitner et al., 2012; Liou and Willison, 1997; Lopez et al., 2015). The structure is known as the Tailless Complex Protein-1 (TCP-1) Ring Complex (TRiC); also known as Complex Containing TCP-1 (CCT) (Lopez et al., 2015). Although originally identified as mediating folding of actin and tubulin (Gao et al., 1992; Sternlicht et al., 1993; Vinh and Drubin, 1994; Yaffe et al., 1992), the TRiC/CCT complex is estimated to interact with ~7% of cytosolic proteins (Yam et al., 2008), although it is not yet clear which of these proteins interact with the TRiC/CCT complex for maturation, refolding, or other processes (Brackley and Grantham, 2009; Lopez et al., 2015).

The high-throughput immunoprecipitation approach (Lowe et al., 2014) was unable to discriminate between direct and indirect protein interactions. To determine if MTGO and *Drosophila* CCT3 interact directly we tested for binding of full-length radiolabeled MTGO protein, synthesized in a coupled in vitro transcription and translation (TNT) system, with bacterially expressed N-terminal GST-tagged full-length CCT3 (GST-CCT3), or with GST alone as a negative control (Fig. 7A). As shown (Fig. 7B), full-length MTGO (1–1762) bound to CCT3. Although weak, the binding appeared specific because only trace sedimentation of MTGO occurred when GST was used instead of the GST-CCT3 fusion protein. To verify this interaction, and to identify which region(s) of MTGO is required for binding to CCT3, we tested interaction of full-length CCT3 with several different truncation variants of MTGO. Several important results emerged from this analysis (Fig. 7). First, residues 1–1020 of MTGO (containing the Proline Rich Region (PRR) and the first

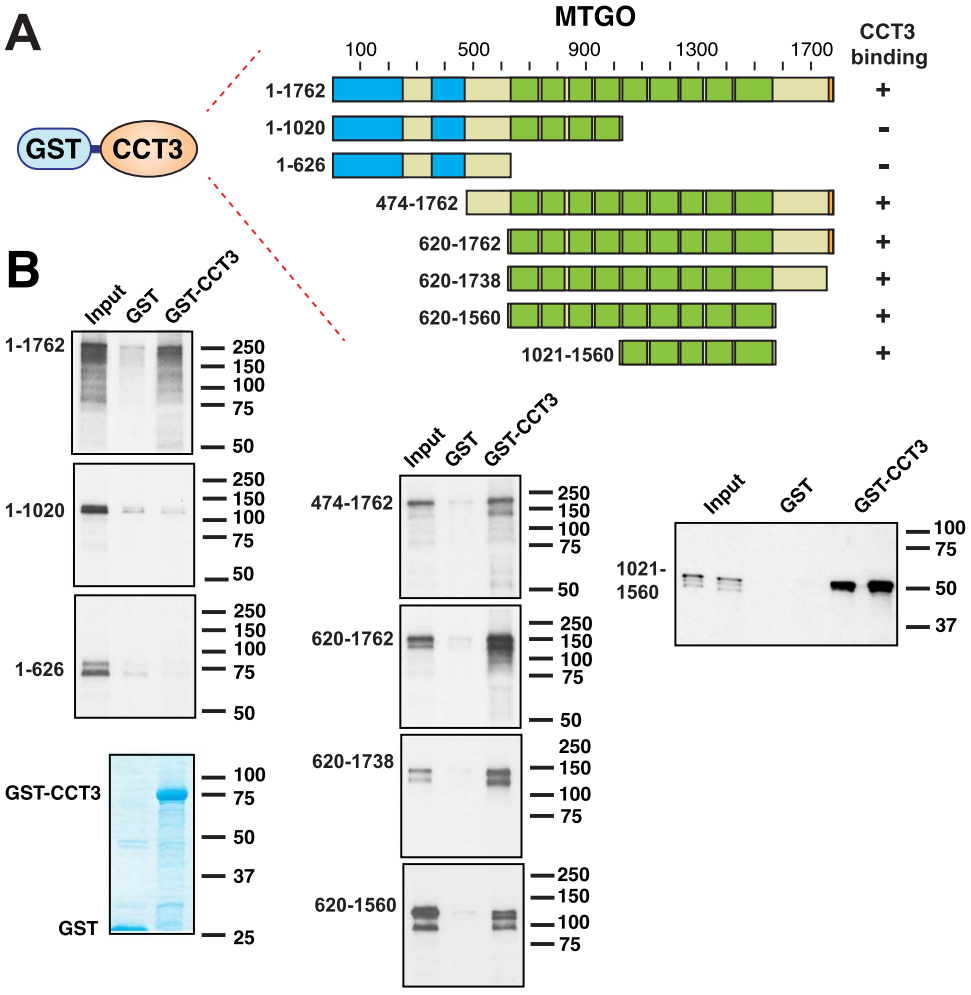

Fig. 7. Physical interaction between MTGO and CCT3. (**A**) *D. melanogaster* full-length CCT3 coding sequence fused to GST was tested for binding to either full-length or truncated/deleted derivatives of MTGO. Qualitative results of these experiments are shown on the right: '+' indicates binding; '–' indicates no binding above background binding to GST alone. The two blue boxes denote regions of low sequence complexity within the PRR, the nine darker green boxes represent the FN3 domains, and the small orange box at the C-terminus represents the tail-anchoring domain.(**B**) A region within the last five FN3 domains of MTGO is necessary and sufficient for binding to GST-CCT3. Each gel was analyzed by staining with GelCode Blue for visualization of the bound GST fusion protein (a representative stained gel is shown for 1–1762 analysis) followed by exposure to a phospho-storage screen for visualization of the bound radiolabeled protein. Results shown are representative of at least three independent experiments.

four FN3 domains) were neither necessary nor sufficient for binding to CCT3. Second, the hydrophobic C-terminal tail-anchoring domain was not required for CCT3 binding. Third, residues 1021–1560 were both necessary and sufficient for binding to CCT3. In summary, MTGO binds directly to CCT3, and a region(s) within the last five FN3-domains in MTGO is necessary and sufficient for this interaction.

3.10. Heterozygous mutant CCT3 larvae display NMJ defects and CCT3 interacts genetically with mtgo

Drosophila mutant in *CCT3* (previously known as *vine* (*vin*)) were first isolated in a screen for genes required for tracheal branching (Ghabrial et al., 2011). Because of the direct interaction between MTGO and CCT3, we investigated whether *CCT3* might also be required for NMJ formation. Although homozygous $CCT3^{512}$ mutants are embryonic lethal, $CCT3^{512}$ heterozygotes are viable (Ghabrial et al., 2011). Indeed, analysis of heterozygous $CCT3^{512}$ third-instar larvae showed abnormalities in muscle 6/7 NMJ similar to those found in $mtgo^{e02963}$ homozygotes (e.g., compare Fig. 8B with Fig. 3D). The defects observed in the NMJ of $CCT3^{512}$ heterozygotes are due to mutations in the *CCT3* locus, and are not a consequence of second-site mutations from the screen, as demonstrated by the ability of a transgenic copy of the *CCT3* genomic locus to rescue both the disrupted NMJ and lethality phenotypes in $CCT3^{512}$ homozygotes (Fig. 8C).

We next investigated whether *mtgo* and *CCT3* showed genetic interaction by comparing the survival of $mtgo^{e02963}$/+; +/$CCT3^{512}$ flies to control *actGFP/+; +/*$CCT3^{512}$ animals (Fig. 8D). We observed synthetic lethality in the $mtgo^{e02963}$/+; +/$CCT3^{512}$ double heterozygote flies, with survival of $mtgo^{e02963}$/+; +/$CCT3^{512}$ flies being reduced to 48% of expected at 25 °C, with a further reduction in viability (36%) in animals propagated at 29 °C (Fig. 8D). As a control, we performed a similar analysis with flies carrying a null mutation in *wishful thinking (wit)*, which encodes a type-II BMP receptor required for NMJ development (Marques et al., 2002; Marqués et al., 2003). In contrast, no genetic interaction was observed for $mtgo^{e02963}$ and *wit* in this assay (Fig. 8D). This result demonstrates that CCT3 and MTGO are both required for terminal axon branching and NMJ growth in *Drosophila* and supports that they do so in a synergistic manner.

3.11. CCT3 G297D encoded by $CCT3^{512}$ exhibits diminished binding to MTGO

All CCT subunits have a common architecture comprised of a conserved equatorial ATP-binding domain and an apical domain that binds substrates (Joachimiak et al., 2014). The only difference between wild-type *CCT3* and the $CCT3^{512}$ allele is a single G297D missense

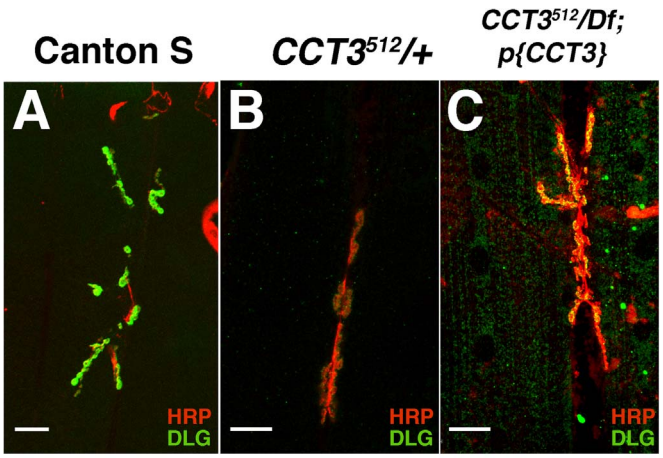

D

Cross 1 *mtgo/actGFP; +/+ x +/+; CCT3/TM3*

	mtgo/+; +/CCT3	*actGFP/+; +/CCT3*	*mtgo/+; +/TM3*	*actGFP/+; +/TM3*	*mtgo/+; +/CCT3* % survival *
25°C	48	101	57	58	48 %
29°C	27	76	40	41	36 %

Cross 2 *mtgo/CyOGFP; +/+ x +/+; wit/TM6B*

	mtgo/+; +/wit	*CyOGFP/+; +/wit*	*mtgo/+; +/TM6B*	*CyOGFP/+; +/TM6B*	*mtgo/+; +/wit* % survival *
25°C	83	79	73	70	105 %

Fig. 8. NMJ defect in $CCT3^{512}$/+ larvae and genetic interaction between *CCT3* and *mtgo*. (**A-C**) Analysis of NMJ in muscle 6/7 in (A) Canton S, (B) $CCT3^{512}$ /+ and (C) $CCT3^{512}$ /+ ; *p{CCT3}* third-instar larvae. Combined images of HRP (red) and DLG (green) immunostaining are shown. See Supplemental Fig. 6 for individual channels. Note the similarity in NMJ phenotype in $CCT3^{512}$ /+ animals (B) compared with $mtgo^{e02963}$ homozygotes (Fig. 3D). Scale bars 20 μm. (**D**) Genetic interaction between *mtgo* and *CCT3*. The table shows the number of animals of each genotype generated from the two different crosses. *- percentage survival of $mtgo^{e02963}$/+; +/$CCT3^{512}$ animals is calculated relative to the control *actGFP/+; +/* $CCT3^{512}$ genotype animals. Similarly, relative survival of $mtgo^{e02963}$*; +/wit* animals was compared with *CyOGFP/+; +/wit* animals. The reduction in numbers of offspring with the TM3 and TM6B balancers is due to reduced fitness associated with these chromosomes in this analysis. Number of independent experiments were two for each temperature in Cross 1 and one for Cross 2. See Materials and Methods for full genotypes of crosses performed.

mutation (Fig. 9A) (Ghabrial et al., 2011). This substitution is located in a conserved region immediately N-terminal of a helical domain (H11) that contributes to the architecture of the substrate binding region (Joachimiak et al., 2014). We tested whether the CCT3 G297D mutation could affect the direct binding of CCT3 to MTGO by testing a G297D-substituted version of GST-CCT3 in our in vitro binding assay (Fig. 9B). For these experiments, three MTGO derivatives containing the CCT3 binding domain but lacking the N-terminal portion of MTGO were used because the truncated constructs had provided the most robust expression in previous experiments. As before, wild-type CCT3 bound efficiently to all three MTGO derivatives (Fig. 9C). In contrast, $CCT3_{G297D}$ displayed substantially reduced binding to the same MTGO derivatives (Fig. 9C). Binding of $CCT3_{G297D}$ to both $MTGO_{620–1738}$ and $MTGO_{620–1560}$ was similarly reduced (Fig. 9C). Quantification showed that $CCT3_{G297D}$ bound to $MTGO_{620–1762}$ at ~40% the level of wild-type CCT3 (Fig. 9D). Thus, the $CCT3^{512}$ mutant synergizes with the *mtgo* mutant genetically and disrupts physical interaction between MTGO and CCT3.

4. Discussion

This is the first report of the function of *CG42389* (*mtgo*) in *Drosophila*. *Mtgo* encodes homologs of vertebrate intracellular cytosolic membrane-anchored FNDC3 proteins, and its expression is required in neurons for NMJ development. Loss of MTGO severely reduces larval NMJ growth and arborization. MTGO interacts both physically and genetically with *CCT3*, which encodes a subunit of the TRiC/CCT chaperonin complex that controls maturation and re-folding of many cytosolic proteins, including actin and tubulin (Lopez et al., 2015; Yam et al., 2008). The $CCT3^{512}$ G297D mutation in *Drosophila* reduced binding of CCT3 to MTGO, and heterozygous $CCT3^{512}$ mutant larvae displayed abnormal NMJ development that phenocopied *mtgo* homozygotes. Taken together, a plausible model for function of MTGO is to localize CCT3 and, by extension, potentially the entire TRiC/CCT complex, to a cytosolic juxta-membrane location where chaperonin activity is required to mediate growth and branching of the NMJ.

4.1. MTGO and CCT3 are required for Drosophila NMJ development

Genetic studies have demonstrated that many factors can influence NMJ size and morphology during development in a dose-dependent manner, including components of signaling pathways (e.g. the Transforming Growth Factor β (TGFβ) superfamily ligand glass bottom boat (GBB) and the Wnt family morphogen Wingless (WG)), proteins involved in cytoskeletal function (e.g., Futsch, Dia, Trio, DVAP-33), components of the ubiquitin-proteasome system (e.g. Highwire (Hiw), Fat facets (Faf)), elements of the autophagy system (Atg) (Shen and Ganetzky, 2009), and other loci (Valakh et al., 2012), see (Menon et al., 2013) for review. In principle, modulating the expression of such genes during normal development provides a mechanism for organisms to incrementally adjust the size of an NMJ endplate to that appropriate for the size of its target muscle. The current study identifies two additional factors, MTGO and CCT3 , which are required for NMJ development. Our data also support the possibility that both proteins function in a dose-dependent manner for NMJ development, although additional studies are required to verify this prediction. Our studies suggest that MTGO expression may be rate-limiting for the formation of boutons, particularly at larval muscle 6/7. As shown (Fig. 4A,D), modest overexpression of *mtgo* produced more boutons compared to WT animals and there was also a trend for increased branches compared to WT control animals. By contrast, higher expression of *mtgo*, mediated by a relatively strong *actin > GAL4* driver, invariably resulted in lethality (Fig. 4C).

4.2. MTGO is required within the nervous system for normal development

At the *Drosophila* NMJ, signals are required from both the neuron and the target muscle to elaborate and maintain the synapse. Anterograde signaling from neuron to muscle is largely mediated by WG (Koles and Budnik, 2012) while retrograde signaling from the muscle is mostly mediated by GBB (Marqués, 2005). We compared the effect of mutation of *mtgo* on NMJ development with the effects of mutations in the *wg* and *gbb* pathways. Loss of WG signaling leads to a modest reduction in the number of boutons, but unlike boutons in *mtgo* mutants, boutons in *wg* mutants are enlarged and irregularly shaped (Packard et al., 2002; Miech et al., 2008). Overall, the severity of the NMJ phenotype in homozygous mutant *mtgo* larvae resembles that observed in mutants with defects in WG or GBB signaling. The increased number of ghost boutons in *mtgo* mutants, combined with the fact that *mtgo* activity in neurons, but not muscle, can rescue *mtgo* mutants, suggests that *mtgo* is required presynaptically for development of boutons and for growth and arborization of the NMJ. However, it is important to note that the specific cell type in which *mtgo* function is required for NMJ development is not yet clear. This could be within neuroendocrine cells, perhaps being required for secretion of various neuropeptides, or could be in motoneurons, or might be required in both or even alternative (e.g. glial) cell types.

MTGO is also required for processes other than NMJ branching and growth. Behavioral studies indicate certain neuronal-associated path-

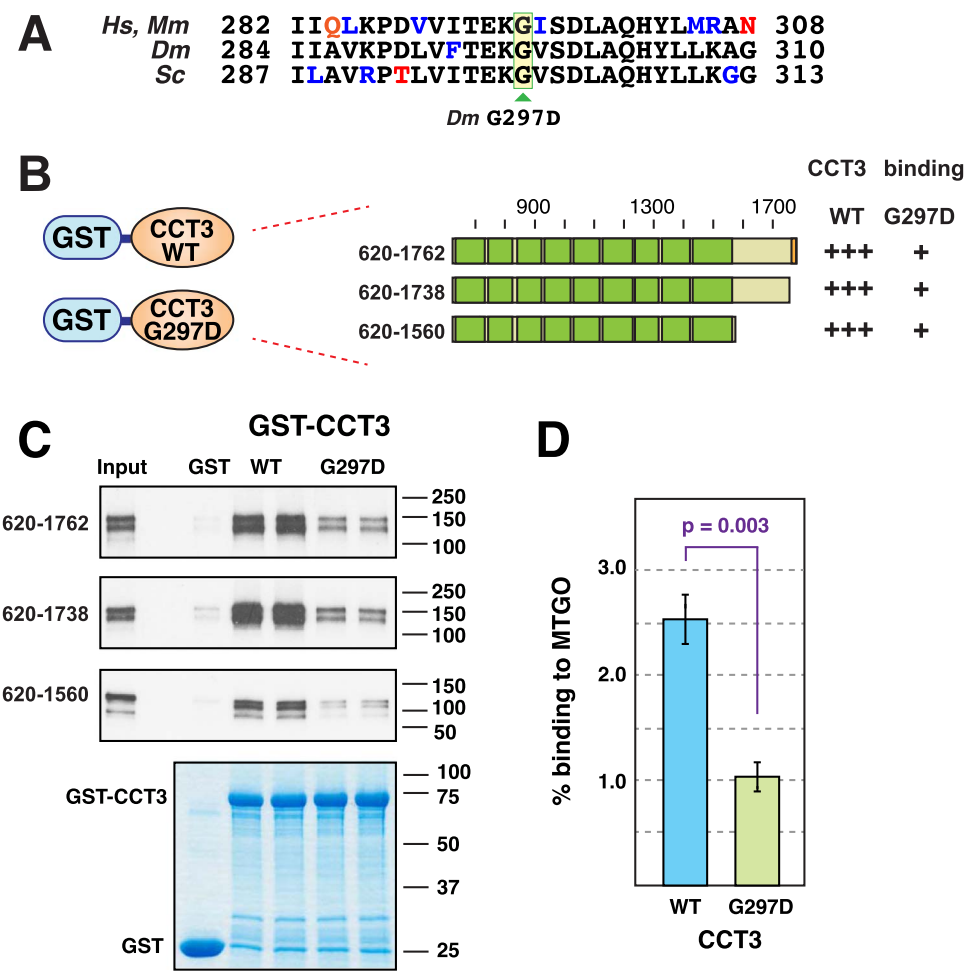

Fig. 9. Reduced binding of MTGO to CCT3 G297D. (**A**) Alignment of the amino acid sequence of a region centered around residue G297 in *D. melanogaster* (*Dm*) CCT3 (Accession number NP_650572, residues shown are 284–310) with corresponding regions from human (*Hs*, NP_005989, residues 282–308), mouse (*Mm*, NP_033966, residues 282–308) and budding yeast (*Sc*, NP_012520, residues 287–313) CCT3 proteins. The human and mouse sequences are identical in this region. Residues identical in all four proteins are colored black; conservative substitutions are blue, non-conserved substitutions are red. G297 and corresponding residues are boxed.(**B**) Wild-type or the G297D variant of *Drosophila* CCT3 fused to GST were tested for binding to the three MTGO derivatives shown. Qualitative results of these experiments are shown on the right: '+++' indicates efficient binding; '+' indicates weaker binding. (**C**) Representative results of binding assays. For each gel, from left to right, input was loaded in lane 1, lane 2 was left blank, and the binding assay results were loaded in lanes 3–7. The bottom panel shows the stained GST fusion proteins.(**D**) Quantification of binding of wild-type (WT) or the G297D mutant of CCT3 to $MTGO_{620-1762}$. Results are the average of four independent repetitions of the binding assay shown in *B* and *C*, with duplicate points (i.e. technical replicates) in each repetition. *Standard error* bars are shown (n = 4). The null hypothesis that the two distributions are the same can be rejected with high confidence ($p = 0.003$, Welch's unequal variance *t*-test with two tails).

ways (e.g. olfaction, proprioception, self-righting) are also affected by loss of MTGO, although others appeared unaffected (e.g. light avoidance, general larval locomotion) suggesting that loss of MTGO may not affect the function of all neuronal types equally. Despite the similar phenotype at muscle 6/7 NMJ in $CCT3^{512}$ heterozygous mutant larvae, the $CCT3^{512}$ mutants were phenotypically wild-type for both self-righting and eclosion, suggesting that these defects in *mtgo* mutants are not due to problems in NMJ development.

4.3. Genetic and physical interaction of MTGO with CCT3

The results of this study suggest that MTGO and CCT3 are components of a novel molecular complex in vivo and demonstrate that both are required in *Drosophila* for terminal axon arborization of the NMJ. We determined that mutants of *mtgo* and *CCT3* (Ghabrial et al., 2011) interact genetically, that MTGO and CCT3 interact physically in vitro, and that the missense $CCT3^{512}$ mutant reduces binding of CCT3 to MTGO. It would be of interest to investigate whether lethality due to overexpression of MTGO is dependent upon the ability of MTGO to bind to CCT3. Our findings support and extend a previous study involving a protein-interaction screen that identified CCT3 as a possible interaction partner with MTGO in vivo (Lowe et al., 2014). Our results are also consistent with two RNAi-based screens that identified a subset of TRiC/CCT-complex-encoding genes as being required for NMJ development (Valakh et al., 2012) (Raut et al., 2017). The fact that independent RNAi of multiple CCTs resulted in similar NMJ phenotypes supports the concept that MTGO may have to interact with the entire TRiC/CCT complex in order for TRiC/CCT to properly influence NMJ development and/or maintenance.

Several reasons suggest interaction of CCT3 with MTGO is unlikely to be required for correct folding of MTGO's FN3 domain(s). Although the TRiC/CCT interactome in human fibroblast cells is enriched in β-strand containing proteins (Yam et al., 2008), FNDC3 proteins were not detected in interaction screens despite the presence of β strands in their FN3 domains (Craig et al., 2004). Furthermore, CCT3 is unable to interact with the first four FN3 domains in MTGO (Fig. 7), making it less likely that CCT3 or TRiC/CCT is required in general for folding of FN3 domains. Instead, we favor a model where interaction of MTGO with CCT3 allows cytoplasmic juxtamembrane localization of CCT3, and by extension possibly the entire CCT/TRiC complex, to enable NMJ development. The cellular and subcellular location of MTGO required for NMJ formation is currently unclear.

FN3 domains are a relatively ancient protein domain found throughout metazoa (King et al., 2008). They are related to immuno-

globulin domains and are found in approximately 2% of all animal proteins (Bork and Doolittle, 1992). The last five FN3 domains of MTGO are sufficient for binding to CCT3 while the first four are not. Because FN3 domains display a relatively low degree of sequence conservation (Craig et al., 2004) it is plausible that the FN3 repeats in MTGO are not functionally equivalent, at least with respect to binding of CCT3, and that a specific region within the last five FN3 domains is required for interaction with CCT3. The ~60% reduction in MTGO - CCT3 binding caused by a single point mutation in CCT3 supports this hypothesis. An important future goal is to define the amino acids in MTGO required for interaction of FNDC3 proteins with CCT3 and to determine whether this region is conserved in other intracellular FN3 domain-containing proteins that might also interact with CCT3 and, by extension, the TRiC/CCT complex. Given MTGO's relatively large size, it is plausible that it could serve as a scaffold to bind other proteins, some of which might require interaction with the TRiC/CCT complex for their maturation and function.

4.4. How does MTGO function in NMJ development ?

How might MTGO and CCT3 function in NMJ growth and branching? In *Drosophila*, live-imaging revealed that NMJ axonal branches arise from pre-existing boutons to form collateral or end branches (Zito et al., 1999). A broad range of proteins are required within the neuron for NMJ arborization and bouton formation including actin, tubulin and regulators of their dynamics (reviewed in Menon et al. (2013)). Because the defect in NMJ arborization in *mtgo* mutants is severe, it is possible that the abnormal branching and growth at the motoneuron terminal might be due to loss of MTGO function affecting multiple different factors within the neuron, either within the cell body or within the axon, or in both locations. Alternatively, loss of MTGO might affect a particularly important key structural component required for NMJ arborization and growth, such as actin. Beta-actin can be supplied via transport of its mRNA to the axon and nerve terminus (reviewed in Eliscovich et al. (2013)). An estimated 1–5% of neuronal actin is synthesized in axons in developing neurons (Eng et al., 1999; Lee and Hollenbeck, 2003). Following translation, nascent actin interacts with two different chaperone complexes, prefoldin (Geissler et al., 1998; Vainberg et al., 1998), then CCT/TRiC (Gao et al., 1992; Sternlicht et al., 1993) to become competent for polymerization. Hence, MTGO within axons might facilitate efficient local maturation of nascent β-actin and refolding of both actin and tubulin required for NMJ endplate branching and growth. Consistent with this model, the TRiC/CCT complex along with Hsc73 and actin, has been localized within axons (Bourke et al., 2002). Similarly, CCT subunits have also been co-localized with actin at the leading edge of developing neurites and migrating fibroblasts (Roobol et al., 1995) where their presence could increase the availability of polymerization-competent actin and tubulin.

Alternatively, MTGO activity might function in the cell body for NMJ growth and branching. Autophagy promotes synapse development in *Drosophila* (Shen and Ganetzky, 2009) and autophagosome function is orchestrated by the actin cytoskeleton in a juxta-membrane location and requires CCT integrity (Pavel et al., 2016). Hence, a MTGO-TRiC/CCT complex might be required to mediate autophagy of select targets by regulating actin dynamics in proximity to cytosolic membranes (Kast and Dominguez, 2017). In *mtgo* mutants, altered autophagy might affect levels of transcription factors or other regulatory proteins required to regulate NMJ growth and branching. Future experiments will investigate these and additional models for how MTGO functions in NMJ development and select behaviors in *Drosophila*.

This study raises several questions. Given its relatively large size, what other proteins may interact with MTGO and are any of these also required for maturation of the NMJ or other functions in neurons? In which neurons is MTGO required for NMJ development and is its activity required within the axon or cell body, or both locations for NMJ arborization? Is MTGO required for activity-dependent plasticity or maintenance of the NMJ in adult animals and is binding of CCT3 to MTGO conserved amongst FNDC3 proteins in other species ? Future experiments that address these and related questions should provide better insight into the mechanism of action of MTGO in NMJ arborization and other neuronal functions in *Drosophila* and may illuminate some of the functions of FNDC3 proteins in vertebrates.

Acknowledgements

We thank Amin Ghabrial (Columbia University Medical Center, NY) for the $CCT3^{512}$ mutant and related *Drosophila* stocks and Daisuke Yamamoto (Tohoku University, Sendai, Japan) for the actin > Gal4 driver stock. We thank Kavita Arora, Doug Bornemann, Todd Holmes, Rahul Warrior and two anonymous reviewers for constructive criticism of the manuscript. AJB and LB were supported by NIGMS P50 GM76516; MP, KGW and GRM were supported in part by NICHD HD045913 and NHLBI HL102862; and JLM was supported by NINDS NS045823, all from the NIH. Confocal microscopy was performed using the UC Irvine Optical Biology Core (OBC). The OBC is a Shared Resource funded in part by the Chao Family Comprehensive Cancer Center Support Grant (P30 CA062203) from the National Cancer Institute. Drosophila stocks and plasmids for this study were obtained from the Bloomington Drosophila Stock Center (NIH P40OD018537) and the Drosophila Genomics and Genetic Resources (DGGR), Kyoto Institute of Technology, Japan. DNA clones were obtained from the Drosophila Genomics Resource Center (DGRC), Bloomington, IN, supported by NIH grant P40 OD010949. The Developmental Studies Hybridoma Bank (DSHB) was developed under the auspices of the NICHD and is maintained by the University of Iowa, Dept. of Biological Sciences, Iowa City, IA 52242. The sponsors had no role in the study design; in the collection, analysis and interpretation of data; in the writing of the report; and in the decision to submit the article for publication.

Conflicts of interest

None.

Author contributions

Designed experiments and analyzed and interpreted data - AJB, LB, TL, JLM, GRM, AS and BZ. Executed experiments – AJB, GTD, JG, WJ, TL, AP, CP, EP, JP, MP, TP, YR, AS, KGW, SW, SW and RZ. Wrote and edited the manuscript - LB, GRM and JLM. All authors reviewed the results and approved the final version of the manuscript.

Appendix A. Supporting information

Supplementary data associated with this article can be found in the online version at doi:10.1016/j.ydbio.2018.10.016.

References

Ataman, B., Ashley, J., Gorczyca, D., Gorczyca, M., Mathew, D., Wichmann, C., Sigrist, S.J., Budnik, V., 2006. Nuclear trafficking of Drosophila Frizzled-2 during synapse development requires the PDZ protein dGRIP. Proc. Natl. Acad. Sci. USA 103, 7841–7846. http://dx.doi.org/10.1073/pnas.0600387103.

Atwood, H.L., Govind, C.K., Wu, C.F., 1993. Differential ultrastructure of synaptic terminals on ventral longitudinal abdominal muscles in Drosophila larvae. J. Neurobiol. 24, 1008–1024. http://dx.doi.org/10.1002/neu.480240803.

Bardwell, A.J., Flatauer, L.J., Matsukuma, K., Thorner, J., Bardwell, L., 2001. A conserved docking site in MEKs mediates high-affinity binding to MAP kinases and cooperates with a scaffold protein to enhance signal transmission. J. Biol. Chem. 276, 10374–10386. http://dx.doi.org/10.1074/jbc.M010271200.

Bardwell, A.J., Frankson, E., Bardwell, L., 2009. Selectivity of docking sites in MAPK kinases. J. Biol. Chem. 284, 13165–13173. http://dx.doi.org/10.1074/jbc.M900080200.

Bardwell, L., Shah, K., 2006. Analysis of mitogen-activated protein kinase activation and interactions with regulators and substrates. Methods 40, 213–223. http://dx.doi.org/10.1016/j.ymeth.2006.06.008.
Bellen, H.J., Tong, C., Tsuda, H., 2010. 100 years of Drosophila research and its impact on vertebrate neuroscience: a history lesson for the future. Nat. Publ. Group 11, 514–522. http://dx.doi.org/10.1038/nrn2839.
Berger, C., Harzer, H., Burkard, T.R., Steinmann, J., van der Horst, S., Laurenson, A.-S., Novatchkova, M., Reichert, H., Knoblich, J.A., 2012. FACS purification and transcriptome analysis of drosophila neural stem cells reveals a role for Klumpfuss in self-renewal. CellReports 2, 407–418. http://dx.doi.org/10.1016/j.celrep.2012.07.008.
Bischof, J., Maeda, R.K., Hediger, M., Karch, F., Basler, K., 2007. An optimized transgenesis system for Drosophila using germ-line-specific phiC31 integrases. Proc. Natl. Acad. Sci. USA 104, 3312–3317. http://dx.doi.org/10.1073/pnas.0611511104.
Bodily, K.D., Morrison, C.M., Renden, R.B., Broadie, K., 2001. A novel member of the Ig superfamily, turtle, is a CNS-specific protein required for coordinated motor control. J. Neurosci. 21, 3113–3125.
Bork, P., Doolittle, R.F., 1992. Proposed acquisition of an animal protein domain by bacteria. Proc. Natl. Acad. Sci. USA 89, 8990–8994.
Bourke, G.J., Alami, El, W., Wilson, S.J., Yuan, A., Roobol, A., Carden, M.J., 2002. Slow axonal transport of the cytosolic chaperonin CCT with Hsc73 and actin in motor neurons. J. Neurosci. Res. 68, 29–35. http://dx.doi.org/10.1002/jnr.10186.
Brackley, K.I., Grantham, J., 2009. Activities of the chaperonin containing TCP-1 (CCT): implications for cell cycle progression and cytoskeletal organisation. Cell Stress Chaperon. 14, 23–31. http://dx.doi.org/10.1007/s12192-008-0057-x.
Cai, C., Rajaram, M., Zhou, X., Liu, Q., Marchica, J., Li, J., Powers, R.S., 2012. Activation of multiple cancer pathways and tumor maintenance function of the 3q amplified oncogene FNDC3B. Cell Cycle 11, 1773–1781. http://dx.doi.org/10.4161/cc.20121.
Cao, Y., Mitchell, E.B., Gorski, J.L., Hollinger, C., Hoppman, N.L., 2016. Two cases with de novo 3q26.31 microdeletion suggest a role for FNDC3B in human craniofacial development. Am. J. Med. Genet. A. http://dx.doi.org/10.1002/ajmg.a.37892.
Carrouel, F., Couble, M.-L., Vanbelle, C., Staquet, M.-J., Magloire, H., Bleicher, F., 2008. HUGO (FNDC3A): a new gene overexpressed in human odontoblasts. J. Dent. Res. 87, 131–136.
Chen, C.-F., Hsu, E.-C., Lin, K.-T., Tu, P.-H., Chang, H.-W., Lin, C.-H., Chen, Y.-J., Gu, D.-L., Lin, C.-H., Wu, J.-Y., Chen, Y.-T., Hsu, M.-T., Jou, Y.-S., 2010. Overlapping high-resolution copy number alterations in cancer genomes identified putative cancer genes in hepatocellular carcinoma. Hepatology 52, 1690–1701. http://dx.doi.org/10.1002/hep.23847.
Chen, K., Featherstone, D.E., 2005. Discs-large (DLG) is clustered by presynaptic innervation and regulates postsynaptic glutamate receptor subunit composition in Drosophila. BMC Biol. 3, 1. http://dx.doi.org/10.1186/1741-7007-3-1.
Craig, D., Gao, M., Schulten, K., Vogel, V., 2004. Tuning the mechanical stability of fibronectin type III modules through sequence variations. Structure 12, 21–30.
Dettman, R.W., Turner, F.R., Hoyle, H.D., Raff, E.C., 2001. Embryonic expression of the divergent Drosophila beta3-tubulin isoform is required for larval behavior. Genetics 158, 253–263.
Eliscovich, C., Buxbaum, A.R., Katz, Z.B., Singer, R.H., 2013. mRNA on the move: the road to its biological destiny. J. Biol. Chem. 288, 20361–20368. http://dx.doi.org/10.1074/jbc.R113.452094.
Eng, H., Lund, K., Campenot, R.B., 1999. Synthesis of beta-tubulin, actin, and other proteins in axons of sympathetic neurons in compartmented cultures. J. Neurosci. 19, 1–9.
Frydman, J., Nimmesgern, E., Erdjument-Bromage, H., Wall, J.S., Tempst, P., Hartl, F.U., 1992. Function in protein folding of TRiC, a cytosolic ring complex containing TCP-1 and structurally related subunits. EMBO J. 11, 4767–4778.
Gao, Y., Thomas, J.O., Chow, R.L., Lee, G.H., Cowan, N.J., 1992. A cytoplasmic chaperonin that catalyzes beta-actin folding. Cell 69, 1043–1050.
Geissler, S., Siegers, K., Schiebel, E., 1998. A novel protein complex promoting formation of functional alpha- and gamma-tubulin. EMBO J. 17, 952–966. http://dx.doi.org/10.1093/emboj/17.4.952.
Ghabrial, A.S., Levi, B.P., Krasnow, M.A., 2011. A systematic screen for tube morphogenesis and branching genes in the Drosophila tracheal system. PLoS Genet. 7, e1002087. http://dx.doi.org/10.1371/journal.pgen.1002087.
Gho, M., 1994. Voltage-clamp analysis of gap junctions between embryonic muscles in Drosophila. J. Physiol. 481 (Pt 2), 371–383.
Gomez-Marin, A., Louis, M., 2012. Active sensation during orientation behavior in the Drosophila larva: more sense than luck. Curr. Opin. Neurobiol. 22, 208–215. http://dx.doi.org/10.1016/j.conb.2011.11.008.
Gomez-Marin, A., Stephens, G.J., Louis, M., 2011. Active sampling and decision making in Drosophila chemotaxis. Nat. Commun. 2, 441. http://dx.doi.org/10.1038/ncomms1455.
Gordon, E.A., Whisenant, T.C., Zeller, M., Kaake, R.M., Gordon, W.M., Krotee, P., Patel, V., Huang, L., Baldi, P., Bardwell, L., 2013. Combining docking site and phosphosite predictions to find new substrates: identification of smoothelin-like-2 (SMTNL2) as a c-Jun N-terminal kinase (JNK) substrate. Cell Signal. 25, 2518–2529. http://dx.doi.org/10.1016/j.cellsig.2013.08.004.
Guan, B., Hartmann, B., Kho, Y.H., Gorczyca, M., Budnik, V., 1996. The Drosophila tumor suppressor gene, dlg, is involved in structural plasticity at a glutamatergic synapse. CURBIO 6, 695–706.
Halpern, M.E., Chiba, A., Johansen, J., Keshishian, H., 1991. Growth cone behavior underlying the development of stereotypic synaptic connections in Drosophila embryos. J. Neurosci. 11, 3227–3238.
Hoang, B., Chiba, A., 2001. Single-cell analysis of Drosophila larval neuromuscular synapses. Dev. Biol. 229, 55–70. http://dx.doi.org/10.1006/dbio.2000.9983.
Hummel, T., Krukkert, K., Roos, J., Davis, G., Klämbt, C., 2000. Drosophila Futsch/22C10 is a MAP1B-like protein required for dendritic and axonal development. Neuron 26, 357–370.
Ito, K., Awano, W., Suzuki, K., Hiromi, Y., Yamamoto, D., 1997. The Drosophila mushroom body is a quadruple structure of clonal units each of which contains a virtually identical set of neurones and glial cells. Development 124, 761–771.
Jan, L.Y., Jan, Y.N., 1982. Antibodies to horseradish peroxidase as specific neuronal markers in Drosophila and in grasshopper embryos. Proc. Natl. Acad. Sci. USA 79, 2700–2704.
Joachimiak, L.A., Walzthoeni, T., Liu, C.W., Aebersold, R., Frydman, J., 2014. The structural basis of substrate recognition by the eukaryotic chaperonin TRiC/CCT. Cell 159, 1042–1055. http://dx.doi.org/10.1016/j.cell.2014.10.042.
Kast, D.J., Dominguez, R., 2017. The cytoskeleton-autophagy connection. Curr. Biol. 27, R318–R326. http://dx.doi.org/10.1016/j.cub.2017.02.061.
Khurana, S., Siddiqi, O., 2013. Olfactory responses of Drosophila larvae. Chem. Senses 38, 315–323. http://dx.doi.org/10.1093/chemse/bjs144.
Kim, M.D., Wen, Y., Jan, Y.N., 2009. Patterning and organization of motor neuron dendrites in the Drosophila larva. Dev. Biol. 336, 213–221. http://dx.doi.org/10.1016/j.ydbio.2009.09.041.
Kim, Y.-J., Bao, H., Bonanno, L., Zhang, B., Serpe, M., 2012. Drosophila Neto is essential for clustering glutamate receptors at the neuromuscular junction. Genes Dev. 26, 974–987. http://dx.doi.org/10.1101/gad.185165.111.
King, N., Westbrook, M.J., Young, S.L., Kuo, A., Abedin, M., Chapman, J., Fairclough, S., Hellsten, U., Isogai, Y., Letunic, I., Marr, M., Pincus, D., Putnam, N., Rokas, A., Wright, K.J., Zuzow, R., Dirks, W., Good, M., Goodstein, D., Lemons, D., Li, W., Lyons, J.B., Morris, A., Nichols, S., Richter, D.J., Salamov, A., Sequencing, J.G.I., Bork, P., Lim, W.A., Manning, G., Miller, W.T., McGinnis, W., Shapiro, H., Tjian, R., Grigoriev, I.V., Rokhsar, D., 2008. The genome of the choanoflagellate Monosiga brevicollis and the origin of metazoans. Nature 451, 783–788. http://dx.doi.org/10.1038/nature06617.
Kishimoto, K., Nishizuka, M., Katoh, D., Kato, A., Osada, S., Imagawa, M., 2013. FAD104, a regulatory factor of adipogenesis, acts as a novel regulator of calvarial bone formation. J. Biol. Chem. 288, 31772–31783. http://dx.doi.org/10.1074/jbc.M113.452961.
Kishimoto, K., Nishizuka, M., Ueda, T., Kajita, K., Ugawa, S., Shimada, S., Osada, S., Imagawa, M., 2011. Indispensable role of factor for adipocyte differentiation 104 (fad104) in lung maturation. Exp. Cell Res. 317, 2110–2123. http://dx.doi.org/10.1016/j.yexcr.2011.06.003.
Koles, K., Budnik, V., 2012. Wnt signaling in neuromuscular junction development. Cold Spring Harb. Perspect. Biol., 4. http://dx.doi.org/10.1101/cshperspect.a008045.
Lahey, T., Gorczyca, M., Jia, X.X., Budnik, V., 1994. The Drosophila tumor suppressor gene dlg is required for normal synaptic bouton structure. Neuron 13, 823–835.
LaLonde, M., Janssens, H., Yun, S., Crosby, J., Redina, O., Olive, V., Altshuller, Y.M., Choi, S.-Y., Du, G., Gergen, J.P., Frohman, M.A., 2006. A role for Phospholipase D in Drosophila embryonic cellularization. BMC Dev. Biol. 6, 60. http://dx.doi.org/10.1186/1471-213X-6-60.
Landgraf, M., Bossing, T., Technau, G.M., Bate, M., 1997. The origin, location, and projections of the embryonic abdominal motorneurons of Drosophila. J. Neurosci. 17, 9642–9655.
Lane, D.P., Crawford, L.V., 1979. T antigen is bound to a host protein in SV40-transformed cells. Nature 278, 261–263.
Lee, S.-K., Hollenbeck, P.J., 2003. Organization and translation of mRNA in sympathetic axons. J. Cell Sci. 116, 4467–4478. http://dx.doi.org/10.1242/jcs.00745.
Leitner, A., Joachimiak, L.A., Bracher, A., Mönkemeyer, L., Walzthoeni, T., Chen, B., Pechmann, S., Holmes, S., Cong, Y., Ma, B., Ludtke, S., Chiu, W., Hartl, F.U., Aebersold, R., Frydman, J., 2012. The molecular architecture of the eukaryotic chaperonin TRiC/CCT. Structure 20, 814–825. http://dx.doi.org/10.1016/j.str.2012.03.007.
Lin, C.-H., Lin, Y.-W., Chen, Y.-C., Liao, C.-C., Jou, Y.-S., Hsu, M.-T., Chen, C.-F., 2016. FNDC3B promotes cell migration and tumor metastasis in hepatocellular carcinoma. Oncotarget. http://dx.doi.org/10.18632/oncotarget.10374.
Linzer, D.I., Levine, A.J., 1979. Characterization of a 54K dalton cellular SV40 tumor antigen present in SV40-transformed cells and uninfected embryonal carcinoma cells. Cell 17, 43–52.
Liou, A.K., Willison, K.R., 1997. Elucidation of the subunit orientation in CCT (chaperonin containing TCP1) from the subunit composition of CCT micro-complexes. EMBO J. 16, 4311–4316.
Livak, K.J., Schmittgen, T.D., 2001. Analysis of relative gene expression data using real-time quantitative PCR and the 2(-Delta Delta C(T)) Method. Methods 25, 402–408. http://dx.doi.org/10.1006/meth.2001.1262.
Lopez, T., Dalton, K., Frydman, J., 2015. The mechanism and function of group II chaperonins. J. Mol. Biol. 427, 2919–2930. http://dx.doi.org/10.1016/j.jmb.2015.04.013.
Lowe, N., Rees, J.S., Roote, J., Ryder, E., Armean, I.M., Johnson, G., Drummond, E., Spriggs, H., Drummond, J., Magbanua, J.P., Naylor, H., Sanson, B., Bastock, R., Huelsmann, S., Trovisco, V., Landgraf, M., Knowles-Barley, S., Armstrong, J.D., White-Cooper, H., Hansen, C., Phillips, R.G., Drosophila, U.K., Protein Trap Screening Consortium, Lilley, K.S., Russell, S., St Johnston, D.,, 2014. Analysis of the expression patterns, subcellular localisations and interaction partners of Drosophila proteins using a pigP protein trap library. Development 141, 3994–4005. http://dx.doi.org/10.1242/dev.111054.
Marques, G., Bao, H., Haerry, T.E., Shimell, M.J., Duchek, P., Zhang, B., O'Connor, M.B., 2002. The Drosophila BMP type II receptor wishful thinking regulates neuromuscular synapse morphology and function. Neuron 33, 529–543.
Marqués, G., 2005. Morphogens and synaptogenesis in Drosophila. J. Neurobiol. 64, 417–434. http://dx.doi.org/10.1002/neu.20165.
Marqués, G., Haerry, T.E., Crotty, M.L., Xue, M., Zhang, B., O'Connor, M.B., 2003.

Retrograde Gbb signaling through the Bmp type 2 receptor wishful thinking regulates systemic FMRFa expression in Drosophila. Development 130, 5457–5470. http://dx.doi.org/10.1242/dev.00772.
Mazzoni, E.O., Desplan, C., Blau, J., 2005. Circadian pacemaker neurons transmit and modulate visual information to control a rapid behavioral response. Neuron 45, 293–300. http://dx.doi.org/10.1016/j.neuron.2004.12.038.
Menon, K.P., Carrillo, R.A., Zinn, K., 2013. Development and plasticity of the Drosophila larval neuromuscular junction. WIREs Dev. Biol. 2, 647–670. http://dx.doi.org/10.1002/wdev.108.
Miech, C., Pauer, H.-U., He, X., Schwarz, T.L., 2008. Presynaptic local signaling by a canonical wingless pathway regulates development of the Drosophila neuromuscular junction. J. Neurosci. 28, 10875–10884. http://dx.doi.org/10.1523/JNEUROSCI.0164-08.2008.
Nishizuka, M., Kishimoto, K., Kato, A., Ikawa, M., Okabe, M., Sato, R., Niida, H., Nakanishi, M., Osada, S., Imagawa, M., 2009. Disruption of the novel gene fad104 causes rapid postnatal death and attenuation of cell proliferation, adhesion, spreading and migration. Exp. Cell Res. 315, 809–819. http://dx.doi.org/10.1016/j.yexcr.2008.12.013.
Obholz, K.L., Akopyan, A., Waymire, K.G., MacGregor, G.R., 2006. FNDC3A is required for adhesion between spermatids and Sertoli cells. Dev. Biol. 298, 498–513. http://dx.doi.org/10.1016/j.ydbio.2006.06.054.
Packard, M., Koo, E.S., Gorczyca, M., Sharpe, J., Cumberledge, S., Budnik, V., 2002. Drosophila Wnt, wingless, provides an essential signal for pre- and postsynaptic differentiation. Cell 111, 319–330.
Pallos, J., Bodai, L., Lukacsovich, T., Purcell, J.M., Steffan, J.S., Thompson, L.M., Marsh, J.L., 2008. Inhibition of specific HDACs and sirtuins suppresses pathogenesis in a Drosophila model of Huntington's disease. Hum. Mol. Genet. 17, 3767–3775. http://dx.doi.org/10.1093/hmg/ddn273.
Park, D., Veenstra, J.A., Park, J.H., Taghert, P.H., 2008. Mapping peptidergic cells in Drosophila: where DIMM fits in. PLoS One 3, e1896. http://dx.doi.org/10.1371/journal.pone.0001896.
Parnas, D., Haghighi, A.P., Fetter, R.D., Kim, S.W., Goodman, C.S., 2001. Regulation of postsynaptic structure and protein localization by the Rho-type guanine nucleotide exchange factor dPix. Neuron 32, 415–424.
Pavel, M., Imarisio, S., Menzies, F.M., Jimenez-Sanchez, M., Siddiqi, F.H., Wu, X., Renna, M., O'Kane, C.J., Crowther, D.C., Rubinsztein, D.C., 2016. CCT complex restricts neuropathogenic protein aggregation via autophagy. Nat. Commun. 7, 13821. http://dx.doi.org/10.1038/ncomms13821.
Prokop, A., Beaven, R., Qu, Y., Sanchez-Soriano, N., 2013. Using fly genetics to dissect the cytoskeletal machinery of neurons during axonal growth and maintenance. J. Cell Sci. 126, 2331–2341. http://dx.doi.org/10.1242/jcs.126912.
Ranganayakulu, G., Schulz, R.A., Olson, E.N., 1996. Wingless signaling induces nautilus expression in the ventral mesoderm of the Drosophila embryo. Dev. Biol. 176, 143–148. http://dx.doi.org/10.1006/dbio.1996.9987.
Raut, S., Mallik, B., Parichha, A., Amrutha, V., Sahi, C., Kumar, V., 2017. RNAi-mediated reverse genetic screen identified drosophila chaperones regulating eye and neuromuscular junction morphology. G3 7, 2023–2038. http://dx.doi.org/10.1534/g3.117.041632.
Roobol, A., Holmes, F.E., Hayes, N.V., Baines, A.J., Carden, M.J., 1995. Cytoplasmic chaperonin complexes enter neurites developing in vitro and differ in subunit composition within single cells. J. Cell Sci. 108 (Pt 4), 1477–1488.
Roos, J., Hummel, T., Ng, N., Klämbt, C., Davis, G.W., 2000. Drosophila Futsch regulates synaptic microtubule organization and is necessary for synaptic growth. Neuron 26, 371–382.
Ruiz-Canada, C., Budnik, V., 2006. Introduction on the use of the Drosophila embryonic/larval neuromuscular junction as a model system to study synapse development and function, and a brief summary of pathfinding and target recognition. Int. Rev. Neurobiol. 75, 1–31. http://dx.doi.org/10.1016/S0074-7742(06)75001-2.
Ruxton, G.D., 2006. The unequal variance *t*-test is an underused alternative to Student's *t*-test and the Mann–Whitney *U* test. Behav. Ecol.. http://dx.doi.org/10.1093/beheco/ark016.
Schuster, C.M., Davis, G.W., Fetter, R.D., Goodman, C.S., 1996. Genetic dissection of structural and functional components of synaptic plasticity. I. Fasciclin II controls synaptic stabilization and growth. Neuron 17, 641–654.
Shen, W., Ganetzky, B., 2009. Autophagy promotes synapse development in Drosophila. J. Cell Biol. 187, 71–79. http://dx.doi.org/10.1083/jcb.200907109.
Sherwood, N.T., Sun, Q., Xue, M., Zhang, B., Zinn, K., 2004. Drosophila spastin regulates synaptic microtubule networks and is required for normal motor function. PLoS Biol. 2, e429. http://dx.doi.org/10.1371/journal.pbio.0020429.
Sink, H., Whitington, P.M., 1991. Location and connectivity of abdominal motoneurons in the embryo and larva of Drosophila melanogaster. J. Neurobiol. 22, 298–311. http://dx.doi.org/10.1002/neu.480220309.
Song, W., Smith, M.R., Syed, A., Lukacsovich, T., Barbaro, B.A., Purcell, J., Bornemann, D.J., Burke, J., Marsh, J.L., 2013. Morphometric analysis of Huntington's disease neurodegeneration in Drosophila. Methods Mol. Biol. 1017, 41–57. http://dx.doi.org/10.1007/978-1-62703-438-8_3.
Stangeland, B., Mughal, A.A., Grieg, Z., Sandberg, C.J., Joel, M., Nygård, S., Meling, T., Murrell, W., Vik, Mo, E.O., Langmoen, I.A., 2015. Combined expressional analysis, bioinformatics and targeted proteomics identify new potential therapeutic targets in glioblastoma stem cells. Oncotarget.
Sternlicht, H., Farr, G.W., Sternlicht, M.L., Driscoll, J.K., Willison, K., Yaffe, M.B., 1993. The t-complex polypeptide 1 complex is a chaperonin for tubulin and actin in vivo. Proc. Natl. Acad. Sci. USA 90, 9422–9426.
Stewart, B.A., Atwood, H.L., Renger, J.J., Wang, J., Wu, C.F., 1994. Improved stability of Drosophila larval neuromuscular preparations in haemolymph-like physiological solutions. J. Comp. Physiol. A 175, 179–191.
Struhl, K., 1991. Reverse biochemistry: methods and applications for synthesizing yeast proteins in vitro. Methods Enzymol. 194, 520–535.
Tominaga, K., Kondo, C., Johmura, Y., Nishizuka, M., Imagawa, M., 2004. The novel gene fad104, containing a fibronectin type III domain, has a significant role in adipogenesis. FEBS Lett. 577, 49–54. http://dx.doi.org/10.1016/j.febslet.2004.09.062.
Vainberg, I.E., Lewis, S.A., Rommelaere, H., Ampe, C., Vandekerckhove, J., Klein, H.L., Cowan, N.J., 1998. Prefoldin, a chaperone that delivers unfolded proteins to cytosolic chaperonin. Cell 93, 863–873.
Valakh, V., Naylor, S.A., Berns, D.S., DiAntonio, A., 2012. A large-scale RNAi screen identifies functional classes of genes shaping synaptic development and maintenance. Dev. Biol. 366, 163–171. http://dx.doi.org/10.1016/j.ydbio.2012.04.008.
Venken, K.J.T., Schulze, K.L., Haelterman, N.A., Pan, H., He, Y., Evans-Holm, M., Carlson, J.W., Levis, R.W., Spradling, A.C., Hoskins, R.A., Bellen, H.J., 2011. MiMIC: a highly versatile transposon insertion resource for engineering Drosophila melanogaster genes. Nat. Methods 8, 737–743. http://dx.doi.org/10.1038/nmeth.1662.
Vinh, D.B., Drubin, D.G., 1994. A yeast TCP-1-like protein is required for actin function in vivo. Proc. Natl. Acad. Sci. USA 91, 9116–9120.
Wang, J.W., Sylwester, A.W., Reed, D., Wu, D.A., Soll, D.R., Wu, C.F., 1997. Morphometric description of the wandering behavior in Drosophila larvae: aberrant locomotion in Na+ and K+ channel mutants revealed by computer-assisted motion analysis. J. Neurogenet. 11, 231–254.
Whisenant, T.C., Ho, D.T., Benz, R.W., Rogers, J.S., Kaake, R.M., Gordon, E.A., Huang, L., Baldi, P., Bardwell, L., 2010. Computational prediction and experimental verification of new MAP kinase docking sites and substrates including Gli transcription factors. PLoS Comput. Biol. 6, e1000908. http://dx.doi.org/10.1371/journal.pcbi.1000908.
Willison, K.R., Dudley, K., Potter, J., 1986. Molecular cloning and sequence analysis of a haploid expressed gene encoding t complex polypeptide 1. Cell 44, 727–738.
Yaffe, M.B., Farr, G.W., Miklos, D., Horwich, A.L., Sternlicht, M.L., Sternlicht, H., 1992. TCP1 complex is a molecular chaperone in tubulin biogenesis. Nature 358, 245–248. http://dx.doi.org/10.1038/358245a0.
Yam, A.Y., Xia, Y., Lin, H.-T.J., Burlingame, A., Gerstein, M., Frydman, J., 2008. Defining the TRiC/CCT interactome links chaperonin function to stabilization of newly made proteins with complex topologies. Nat. Struct. Mol. Biol. 15, 1255–1262. http://dx.doi.org/10.1038/nsmb.1515.
Yamamoto, S., Jaiswal, M., Charng, W.-L., Gambin, T., Karaca, E., Mirzaa, G., Wiszniewski, W., Sandoval, H., Haelterman, N.A., Xiong, B., Zhang, K., Bayat, V., David, G., Li, T., Chen, K., Gala, U., Harel, T., Pehlivan, D., Penney, S., Vissers, L.E.L.M., de Ligt, J., Jhangiani, S.N., Xie, Y., Tsang, S.H., Parman, Y., Sivaci, M., Battaloglu, E., Muzny, D., Wan, Y.-W., Liu, Z., Lin-Moore, A.T., Clark, R.D., Curry, C.J., Link, N., Schulze, K.L., Boerwinkle, E., Dobyns, W.B., Allikmets, R., Gibbs, R.A., Chen, R., Lupski, J.R., Wangler, M.F., Bellen, H.J., 2014. A drosophila genetic resource of mutants to study mechanisms underlying human genetic diseases. Cell 159, 200–214. http://dx.doi.org/10.1016/j.cell.2014.09.002.
Yoshihara, M., Rheuben, M.B., Kidokoro, Y., 1997. Transition from growth cone to functional motor nerve terminal in Drosophila embryos. J. Neurosci. 17, 8408–8426.
Zhang, B., Koh, Y.H., Beckstead, R.B., Budnik, V., Ganetzky, B., Bellen, H.J., 1998. Synaptic vesicle size and number are regulated by a clathrin adaptor protein required for endocytosis. Neuron 21, 1465–1475.
Zito, K., Parnas, D., Fetter, R.D., Isacoff, E.Y., Goodman, C.S., 1999. Watching a synapse grow: noninvasive confocal imaging of synaptic growth in Drosophila. Neuron 22, 719–729.

Miles to go (*mtgo*) encodes FNDC3 proteins that interact with the chaperonin subunit CCT3 and are required for NMJ branching and growth in *Drosophila*

A. Syed et al

Supplemental Figures

Supplemental Figure 1

Amino acid sequence of MTGO proteins encoded by *CG42389-RE*, *-RF* and *-RG* transcripts

Amino acids unique to each isoform are *italicized*. Amino acids shared by all three isoforms are underlined. The region encoding the nine FN3 domains contained within the last exon is colored green. The predicted tail-anchoring (TA) domain at the C-terminus is in bold text. Amino acids encoded by alternating coding exons are denoted by orange and blue. The region containing the nine FN3 domains (amino acids 627-1539 of the MTGO-PF isoform) shares 33-35% amino acid sequence identity with human and mouse FNDC3A and FNDC3B proteins, and these two proteins are the top BLAST hits when the fly sequence is used to search the human or mouse protein sequence databases. Likewise, MTGO is the top BLAST hit when mammalian FNDC3A/B are used to search the fly protein sequence database. Collectively, these observations support that *mtgo*/*CG42389* encodes the *Drosophila* FNDC3 orthologs.

***D.melanogaster* CG42389-PE (2064aa)**

MAAAVLEINENQLELVCDECDYYGATDTIFIDNSTQTDGYDDDESELKPLKPRLSQIVEEEAEMEGTVKEEMDTQVETNGIQSDSNGVSDV
KTAINGNESIVAEEISEEEPPVEASVPHVVQELVDSDDEVEIDDVTRLAGLTLGMGYARIIDYDNLRIIEHVIESDDEDDNNVAAAGTAAT
SAELQQACHDLVTFIGESYQVIERSGHSREPTATLSVVDNNNNNRSSEVSTNGRGAITDRSKSTRKVHNGLQVNQNASTSATATSSSNSKS
NSSNNTAATSNSSALIKAYKSNLTPLAPPFQPAALKAKQLQQSSLPSGNMSSVTTTTTTALGYTAYEQTTVYYQQQVQQQQQQHPQQQQQL
SPKQQQQQQQQPQQQQPICAQHGGLPHIHGAQLLPVQLIALPPNGVTAAAATAAVAAAAGATVAAAGTPAAAAAGGAAATSLTGAAWPLVE
APIYIDINGEYRSYCPAHGPPAVAVPNGAIGHHPHIHAHPPHTHSHAHPTHSHHAQQQQQQQQQQQQQLHHHHQQHGQHQQHLTPSPVTNV
*NGNIAQAAAAAAASAPRLLLQLDAATVQQQQQQQHQQQQQHQQQQQQQIVAAGKRSKVYR*GPAVQMVSQNRPPPPMPVPVQVPQYVNENGTL
THVMLSPQQYQQLHPGQGHLHPAPFISANGTSHFYTPVAGYPGPGPAGNGPPHYHLPPPPPPQQQQQQPPQQPQQQAPQGPPPPQQQQQQQ
QQVAPPAVQGAPSTGSVGAAQGAPATATATHTHAHSHSHSHAHSHTHPQPHAHSPHSPSPPNYRDERSQRQHNKLLRKLEKQRESNPPHSP
SPRRANELNGHNNNNIPPGVPLPGHLNNHHHAVNHQGRRLPQQHQGQAHQVAQQQQSQARNGNPQHPQRAGSSVGGASSVGTSEDGEDNSS
LAGDDEEEYHRENSIIEQISAIEKPEVIDVTSRAAKIIWESPAIANTVTVDMRQLRYQVLLCDSGKQCKYKSLYQGEAYECIVQDLQPGQD
YLVRLQVHYQKLTGTVSDPTEFRTPPCEPDQPPPPKLVSRTKNSINLRWAAPAANGASIQHYLLEYDEGRMPGQPQKFVELAKIKAKHYVI
GKLQPTTVYSFRLAAVNEAGQSPYSPVASYSTSGNPPPVPKPPQLLASSSSSLKLGWERRAQDGDFLLQLQDAETGHGFLNTYKGTELQTE
CLQLRRASSYQFRLRSENEAGFSPWSPEVSYRTLAERPGRPGKPHAKGKIHGTQFKARWDAPSDSGGAEILCYHLELSAAGPAFERIYSGA
ETEAMCERLQPGTTYALRACCEGPAGQSPYSDIGHVTTEAVPPSAPPPPHCSDPPSPYAALLKLRPPEYNGGAPILEFEAQMRRLEQVQPP
QLVYRGKQTYFVAQDLTPGGMYETQVRAINRIGAGSWSQWMRFTAAAAAPGVPEELRVLVKSATHLGVSWQPPLQENGAPVTSYTLKSASQ
ERKEDDSEEEVKEPPSSEFHNCYQGPQTCAELRNLSPYTRYHFRIQASNSAGTGNSSDVISVCTPAAVPGAPQMQGYEFTAQEVTLNWTQP
AAHGSPICSYNIEYGERTIATPDACTRYTVSGLMPETGYKFRVQAVNAIGAGAFSAYAKLTTQPAPPAPPRLECSGAGHNYIKLKWGENGN
GKVVNSNPSGNGGDFTKYFVEMYVARAKQFQAVYSGTNCMCKVHKLQERSSYTFRIYAHTDRAGDGDYSEEFVFETSATLPANIKPPRVVQ
EGSVCLMELPGQLGMQLTLEWQHSKNSFNDRVEYELQYAVLGAAELEGESLSPKGRSSSSSGSSNGAPINLPNHDYRQLYRGPETKFTIDN
LAAGTCYQFRVCPVRIAAGGELLYGQPSSPLRYQVPSELDPSSATCHHHLHGSTATPAMASSQRSSRKLSAGNGSTNGLHMRSVSASAISG
ASGVGADPVAIGRLQQELSGFNACADPQHHHHHHHHHHHQPCGGGVGGAGGISGATDSHHQHQHHMHHSHHMHHAHHPHTGMGGSSSNSSS
STAAAISSSLAQAGGLRRIVCKVTSLYSNRRRLSDQQK**AVCIVVSFLVGTFLVAMLVNMLR**G

***D.melanogaster* CG42389-PF (1762aa)**

MVRLNVAEQHSSSNNNGNISNSSISNTNGTIITSNNNAGGSCSSTTSSTTSLNSNPASPACTMVMLPAPQQHLLVQQQQQQQQQQQQQQQQP
QQPPPQLQQQHGPQQQQQQQQQQHSPSDGGSSNCSLPASPPLLQQTATPPQGAQIVPPVCALHHPQQQLALMAAMQHHHHLPPPHALHHAP
LPPPPPNLPPPHENGHGGGGSGVAVGGGGISPNGGGGSSASSVSSLSSGSGGSGGQVNGLSNGTNGIAPLPPGQLYIQYPGEFYPPEYYIA
*PHPHEGICPQHPHHPHPHHHQPMCAMSTEY*GPAVQMVSQNRPPPPMPVPVQVPQYVNENGTLTHVMLSPQQYQQLHPGQGHLHPAPFISAN
GTSHFYTPVAGYPGPGPAGNGPPHYHLPPPPPPQQQQQQPPQQPQQQAPQGPPPPQQQQQQQQQQVAPPAVQGAPSTGSVGAAQGAPATATA
THTHAHSHSHSHAHSHTHPQPHAHSPHSPSPPNYRDERSQRQHNKLLRKLEKQRESNPPHSPSPRRANELNGHNNNNIPPGVPLPGHLNNH
HHAVNHQGRRLPQQHQGQAHQVAQQQQSQARNGNPQHPQRAGSSVGGASSVGTSEDGEDNSSLAGDDEEEYHRENSIIEQISAIEKPEVID
VTSRAAKIIWESPAIANTVTVDMRQLRYQVLLCDSGKQCKYKSLYQGEAYECIVQDLQPGQDYLVRLQVHYQKLTGTVSDPTEFRTPPCEP
DQPPPPKLVSRTKNSINLRWAAPAANGASIQHYLLEYDEGRMPGQPQKFVELAKIKAKHYVIGKLQPTTVYSFRLAAVNEAGQSPYSPVAS
YSTSGNPPPVPKPPQLLASSSSSLKLGWERRAQDGDFLLQLQDAETGHGFLNTYKGTELQTECLQLRRASSYQFRLRSENEAGFSPWSPEV
SYRTLAERPGRPGKPHAKGKIHGTQFKARWDAPSDSGGAEILCYHLELSAAGPAFERIYSGAETEAMCERLQPGTTYALRACCEGPAGQSP
YSDIGHVTTEAVPPSAPPPPHCSDPPSPYAALLKLRPPEYNGGAPILEFEAQMRRLEQVQPPQLVYRGKQTYFVAQDLTPGGMYETQVRAI
NRIGAGSWSQWMRFTAAAAAPGVPEELRVLVKSATHLGVSWQPPLQENGAPVTSYTLKSASQERKEDDSEEEVKEPPSSEFHNCYQGPQTC
AELRNLSPYTRYHFRIQASNSAGTGNSSDVISVCTPAAVPGAPQMQGYEFTAQEVTLNWTQPAAHGSPICSYNIEYGERTIATPDACTRYT
VSGLMPETGYKFRVQAVNAIGAGAFSAYAKLTTQPAPPAPPRLECSGAGHNYIKLKWGENGNGKVVNSNPSGNGGDFTKYFVEMYVARAKQ
FQAVYSGTNCMCKVHKLQERSSYTFRIYAHTDRAGDGDYSEEFVFETSATLPANIKPPRVVQEGSVCLMELPGQLGMQLTLEWQHSKNSFN
DRVEYELQYAVLGAAELEGESLSPKGRSSSSSGSSNGAPINLPNHDYRQLYRGPETKFTIDNLAAGTCYQFRVCPVRIAAGGELLYGQPSS
PLRYQVPSELDPSSATCHHHLHGSTATPAMASSQRSSRKLSAGNGSTNGLHMRSVSASAISGASGVGADPVAIGRLQQELSGFNACADPQH
HHHHHHHHHHQPCGGGVGGAGGISGATDSHHQHQHHMHHSHHMHHAHHPHTGMGGSSSNSSSSTAAAISSSLAQAGGLRRIVCKVTSLYSN
RRRLSDQQK**AVCIVVSFLVGTFLVAMLVNML**RG

***D.melanogaster* CG42389-PG(1413aa)**

*MDGSKKTLLIK*ISANGTSHFYTPVAGYPGPGPAGNGPPHYHLPPPPPPQQQQQQPPQQPQQQAPQGPPPPQQQQQQQQQVAPPAVQGAPST
GSVGAAQGAPATATATHTHAHSHSHSHAHSHTHPQPHAHSPHSPSPPNYRDERSQRQHNKLLRKLEKQRESNPPHSPSPRRANELNGHNNN
NIPPGVPLPGHLNNHHHAVNHQGRRLPQQHQGQAHQVAQQQQSQARNGNPQHPQRAGSSVGGASSVGTSEDGEDNSSLAGDDEEEYHRENS
IIEQ*ISAIEKPEVIDVTSRAAKIIWES*PAIANTVTVDMRQLRYQVLLCDSGKQCKYKSLYQGEAYECIVQDLQPGQDYLVRLQVHYQKLTG
TVSDPTEFRTPPCEPDQPPPPKLVSRTKNSINLRWAAPAANGASIQHYLLEYDEGRMPGQPQKFVELAKIKAKHYVIGKLQPTTVYSFRLA
AVNEAGQSPYSPVASYSTSGNPPPVPKPPQLLASSSSSLKLGWERRAQDGDFLLQLQDAETGHGFLNTYKGTELQTECLQLRRASSYQFRL
RSENEAGFSPWSPEVSYRTLAERPGRPGKPHAKGKIHGTQFKARWDAPSDSGGAEILCYHLELSAAGPAFERIYSGAETEAMCERLQPGTT
YALRACCEGPAGQSPYSDIGHVTTEAVPPSAPPPPHCSDPPSPYAALLKLRPPEYNGGAPILEFEAQMRRLEQVQPPQLVYRGKQTYFVAQ
DLTPGGMYETQVRAINRIGAGSWSQWMRFTAAAAAPGVPEELRVLVKSATHLGVSWQPPLQENGAPVTSYTLKSASQERKEDDSEEEVKEP
PSSEFHNCYQGPQTCAELRNLSPYTRYHFRIQASNSAGTGNSSDVISVCTPAAVPGAPQMQGYEFTAQEVTLNWTQPAAHGSPICSYNIEY
GERTIATPDACTRYTVSGLMPETGYKFRVQAVNAIGAGAFSAYAKLTTQPAPPAPPRLECSGAGHNYIKLKWGENGNGKVVNSNPSGNGGD
FTKYFVEMYVARAKQFQAVYSGTNCMCKVHKLQERSSYTFRIYAHTDRAGDGDYSEEFVFETSATLPANIKPPRVVQEGSVCLMELPGQLG
MQLTLEWQHSKNSFNDRVEYELQYAVLGAAELEGESLSPKGRSSSSSGSSNGAPINLPNHDYRQLYRGPETKFTIDNLAAGTCYQFRVCPV
RIAAGGELLYGQPSSPLRYQVPSELDPSSATCHHHLHGSTATPAMASSQRSSRKLSAGNGSTNGLHMRSVSASAISGASGVGADPVAIGRL
QQELSGFNACADPQHHHHHHHHHHHQPCGGGVGGAGGISGATDSHHQHQHHMHHSHHMHHAHHPHTGMGGSSSNSSSSTAAAISSSLAQAG
GLRRIVCKVTSLYSNRRRLSDQQK**AVCIVVSFLVGTFLVAMLVNML**RG

Supplemental Figure 2 Transcripts mapping to *CG42389* (*mtgo*) and location of primers used for RT-PCR.

Upper - Sequence of primers used for RT-PCR analyses in this study. Primers used for amplification of ribosomal protein 49 mRNA were as described (LaLonde et al., 2006).

Lower - The *CG42389* (*mtgo*) locus is on the left arm of chromosome 2 at approximately 16.60 Mb. FlyBase (2017_02 released April 18, 2017) annotates four independent transcripts from this gene; *CG42389 -RE, -RF, -RG and -RH*. We were unable to detect the *-RH* isoform from cDNA generated using mRNA isolated from wild type larvae or adult animals. The predicted size of the mRNA encoded by each transcript is indicated. Three additional genes (*CG5968*, *CG31815* and *CG4631*) are located within the ~120kb *mtgo* locus. Based on the location of these genes relative to the Pbac insertion in the $mtgo^{e02963}$ allele they are unlikely to be affected by insertion of the Pbac-element and have been omitted for clarity. The name and location of primers used in the RT-PCR analysis is denoted by an arrowhead with the primer name adjacent. Open boxes denote non-coding exons (5' or 3' UTR) while filled boxes denote coding sequences. An arrow indicates the predicted location of the promoter for each transcript. The initiator AUG codon in exon 3 of transcript *GC42389-RF* is marked, as is the site of integration of the PBac 49 bases 3' to exon 3 in the *e02963* allele of *CG42389 (mtgo)* and the site of integration of the protein trap EYFP vector in the *CPTI001586* allele.

Supplemental Figure 2

E-for	5'-CGCTGGCAAGCGTAGCAAAG-3'
F-for	5'-TGCGCCATGTCCACGGAATAC-3'
G-for	5'-GCCAGCGTGTATAAGTTGACGTG-3'
Com-for	5'-AAGCAGCGGGAGTCAAATCCCC-3'
E_F-rev	5′-TGCAGTTGCTGGTACTGCTGC-3′
G-rev	5′-CACCGGAGTGTAGAAATGCGAAG
Com-rev	5′-CGTCCTTGATGGTTCACTGCATG-3′
EYFP-for	5′-AACGAGAAGCGCGATCACATGG-3′
EYFP-rev	5′-CTGAACTTGTGGCCGTTTACGTC-3′
rp49 for	5'-TACAGGCCCAAGATCGTGAA-3'
rp49 Rev	5'-TCTCCTTGCGCTTCTTGGA-3'

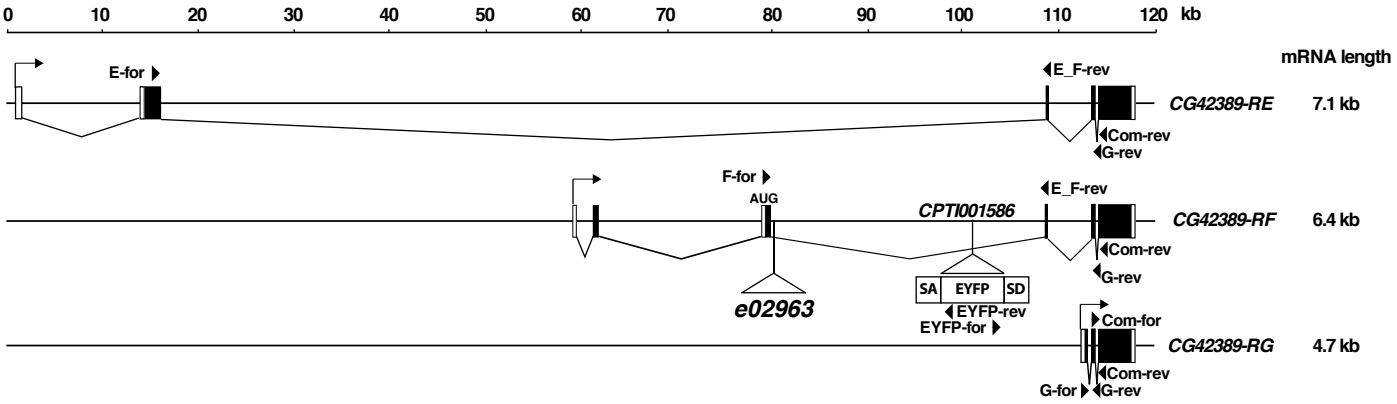

Supplemental Figure 3

RT-PCR and DNA sequencing verifies splicing of *mtgo* exons into EYFP protein trap in larvae homozygous for *mtgo*^{CPTI001586} allele.

(A) RT-PCR analysis of expression of *-RE* and *-RF* transcripts of *mtgo* in Canton S and *mtgo*^{EYFP} homozygous larvae and adult animals. The sequence and binding location of the primers used are shown in Supplemental Fig. 2. Black or white dots to the left side of a lane denote the correct size of the respective PCR products in each gel. The results suggest that the *-RE* isoform is expressed at low levels in larva compared to adults. In contrast, the *-RF* isoform is expressed at similar levels in both larva and adult animals. The results also indicate that relatively little wild-type *-RF* transcript is produced in homozygous *mtgo*^{EYFP} adult animals.

(B) RT-PCR products were gel-purified and sequenced and show correct splicing into and out of the SA-EYFP-SD PIGP681 protein trap vector (Lowe et al., 2014).

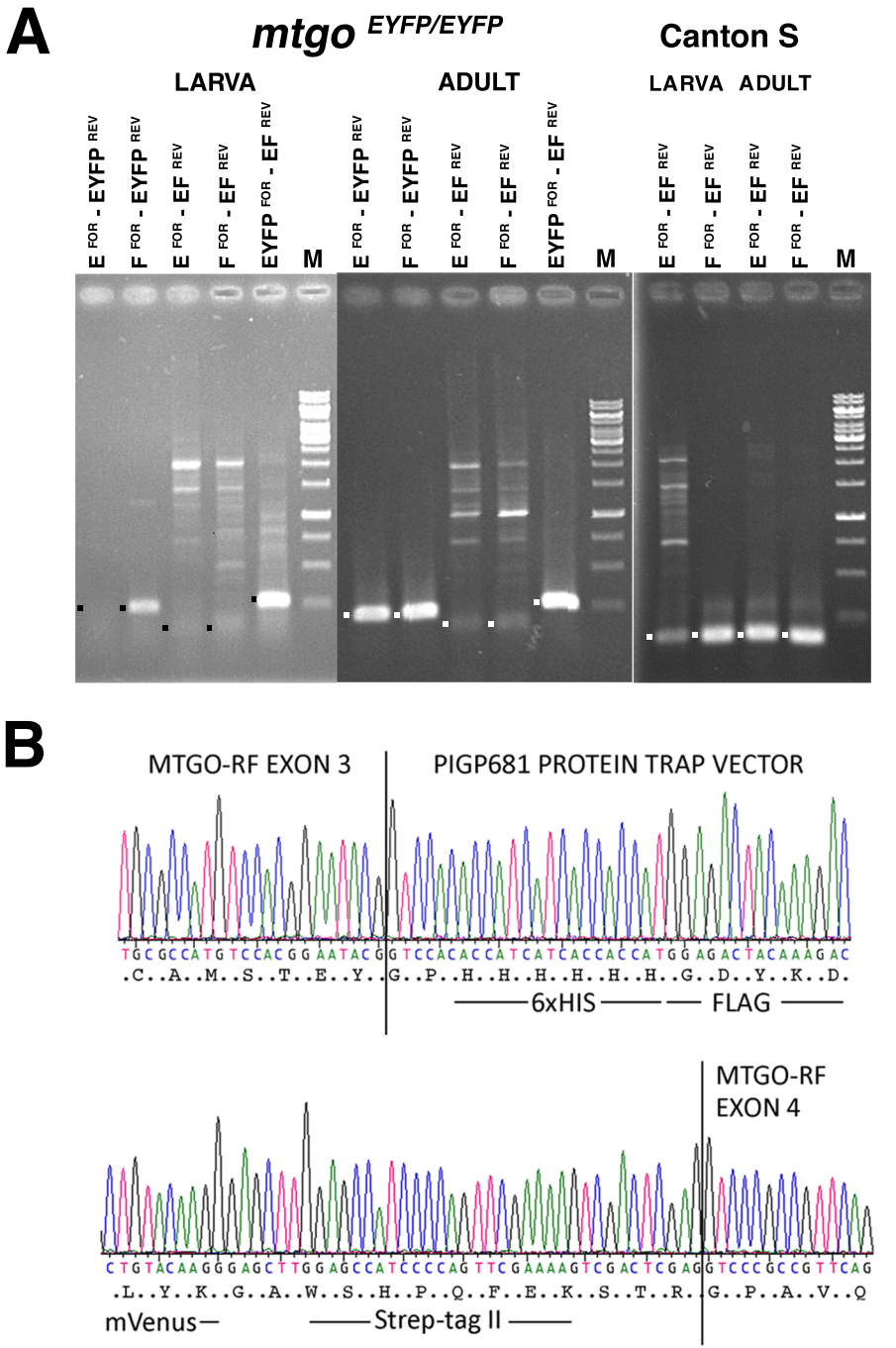
A
mtgo EYFP/EYFP
Canton S
LARVA
ADULT
LARVA
ADULT
E FOR - EYFP REV
F FOR - EYFP REV
E FOR - EF REV
F FOR - EF REV
EYFP FOR - EF REV
M
B
MTGO-RF EXON 3
PIGP681 PROTEIN TRAP VECTOR
TGCGCCATGTCCACGGAATACGGTCCACACCATCATCACCACCATGGAGACTACAAAGAC
.C..A..M..S..T..E..Y..G..P..H..H..H..H..H..H..G..D..Y..K..D.
6xHIS
FLAG
MTGO-RF
EXON 4
CTGTACAAGGGAGCTTGGAGCCATCCCCAGTTCGAAAAGTCGACTCGAGGTCCCGCCGTTCAG
.L..Y..K..G..A..W..S..H..P..Q..F..E..K..S..T..R..G..P..A..V..Q
mVenus
Strep-tag II

Supplemental Figure 4

Expression of MTGO-EYFP fusion protein in homozygous *mtgo*^{EYFP} wandering third-instar larvae.

Dissected CNS and ventral nerve cord from (A-C) homozygous *mtgo*^{EYFP} and (D,E) negative control Canton S wandering third instar larvae were imaged using (A, D) Nomarski / DIC or (B,E) confocal imaging of YFP fluorescence using identical settings for each sample. Panel C shows the images in panels A and B merged. In the nervous system in *mtgo*^{EYFP} animals, very low level EYFP is localized to the CNS in a neuropil glial pattern with broad neuronal localization in the ventral nerve cord (VNC). (F-H) Muscle 6/7 in a homozygous *mtgo*^{EYFP} animal shows fluorescence within the axons (white arrowheads) with a weaker signal in muscle (white arrows). No fluorescence was observed in trachea (e.g. black arrowhead in panel G). Scale bars (A,D) - 85 μm; (F-H) - 50 μm.

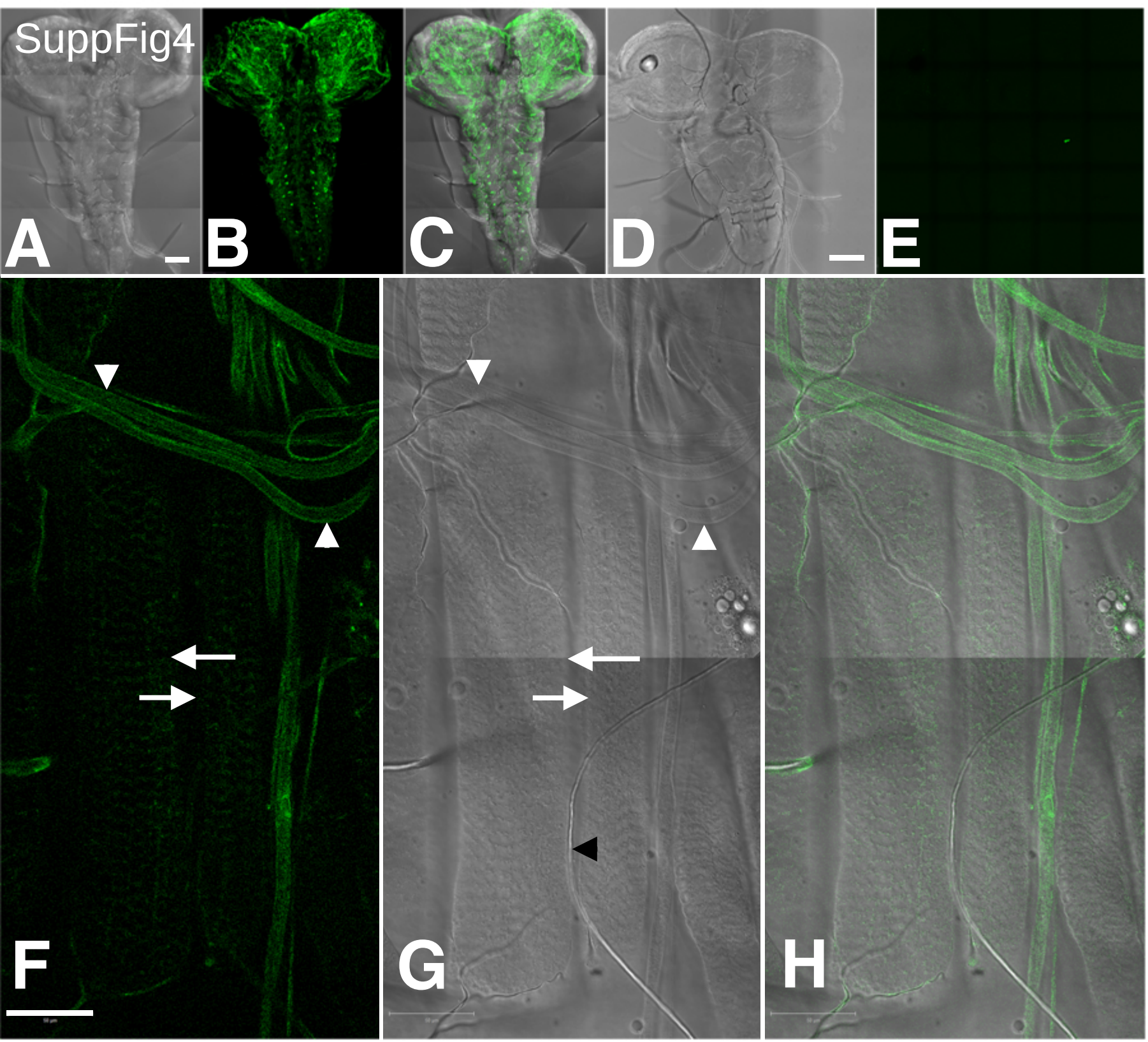
SuppFig4
A
B
C
D
E
F
G
H

Supplemental Figure 5

Analysis of Futsch immunoreactivity in muscle 6/7 NMJ of wild type and homozygous *mtgo*^{e02963} larvae.

Immunostaining of Futsch (green) and neurons (HRP; red) in subsection of muscle 6/7 NMJ of wild-type Canton S (A-C) and homozygous mutant *mtgo*^{e02963} (D-F) third instar wandering larvae. In panels B and E the brightness of the boxed areas has been increased and the image magnified to show examples of weakly staining Futsch loops. Additional loops are indicated by white arrowheads. All scale bars are 3 μm.

Supplemental Figure 5

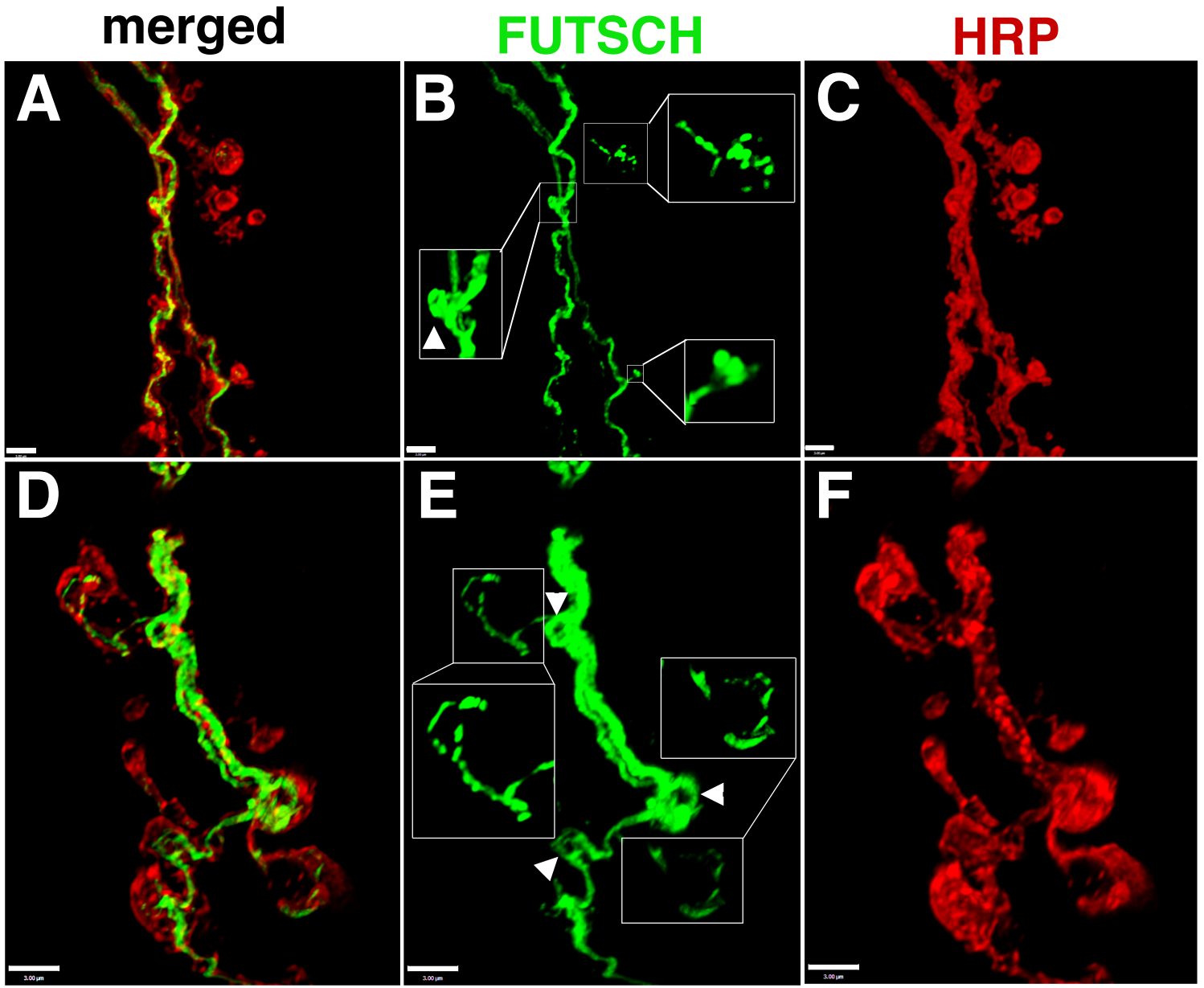

Supplemental Figure 6. NMJ defect in *CCT3^{512}* heterozygous mutant larvae.

Analysis of muscle 6/7 NMJ in (A-C) Canton S, (D-F) *CCT3^{512} /+* and (G-I) *CCT3^{512} /+; p{CCT3}* 3rd instar larvae. The top row is the combined image of HRP (red) and DLG (green) immunostaining shown in Fig. 8. Note the similarity in NMJ phenotype in *CCT^{512} /+* animals in panel D compared with *mtgo^{e02963}* homozygotes (Fig. 3D). Scale bars 20 μm. See Materials and Methods for details of crosses and full genotypes.

Supplemental Figure 6

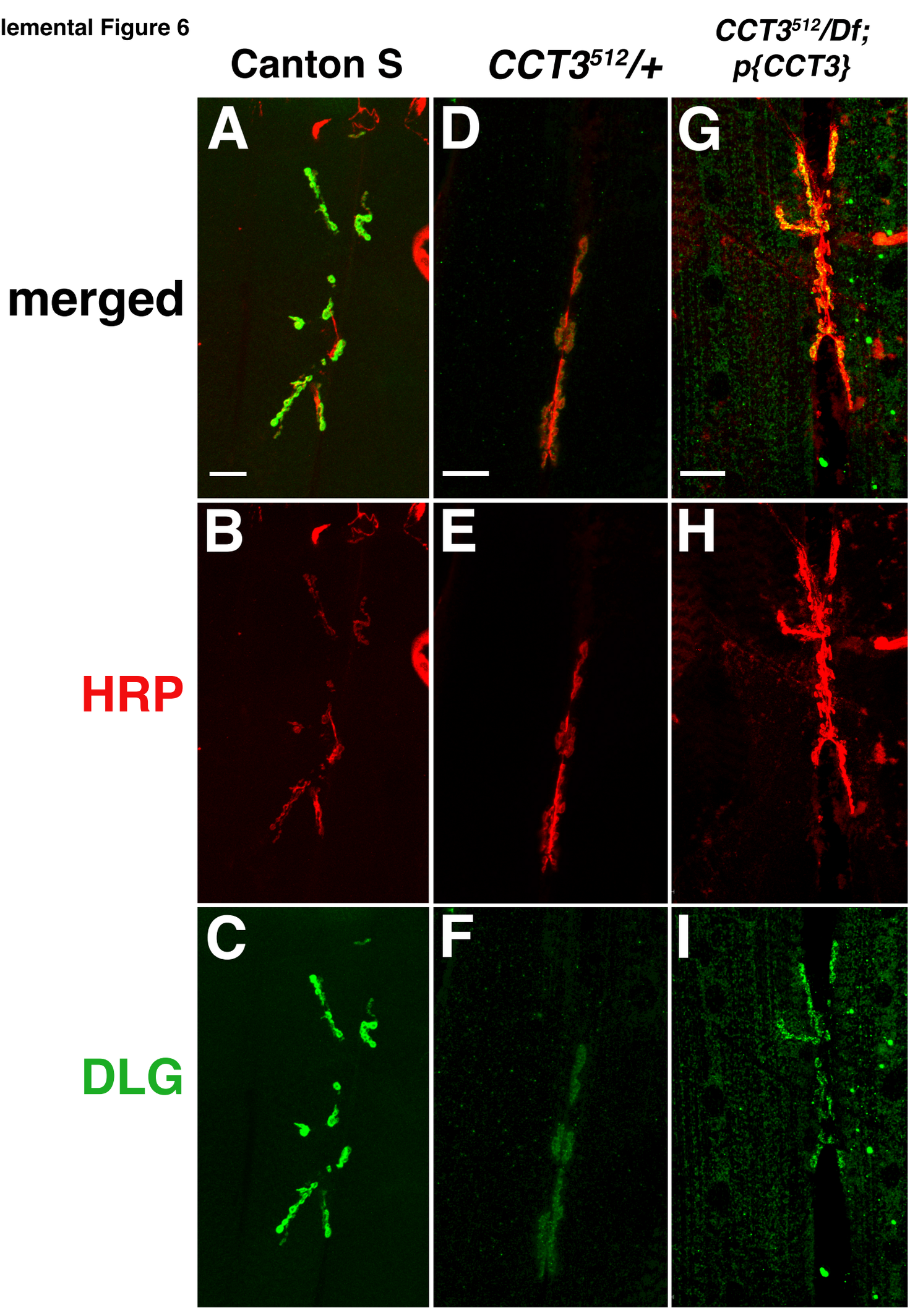

Supplemental Tables

Supplemental Table 1 - Sixty-three proteins in *D. melanogaster* genome containing one or more FN3 domains

Drosophila proteins that contain one or more FN3 domains, the genes encoding them, the types of domains found in each protein, the number of contiguous FN3 domains in each protein and whether the protein has a N-terminal signal peptide sequence. Only one protein is listed for the *CG42389* (*miles to go*, *mtgo*) locus although the locus can encode three different tail-anchored (TA) proteins each containing nine FN3 domains. Thirty-eight out of the 63 proteins have a predicted transmembrane (TM) domain, but only those encoded by *mtgo* have a single TM domain at the extreme end of the C-terminus where it can function as a tail-anchoring domain.

Key to domains (from SMART database) - Ank - ankyrin repeats (SM00248); BBOX - B-Box-type zinc finger (SM00336); BBC - B-Box C-terminal domain (SM00502); CLECT - C-type lectin (CTL) or carbohydrate-recognition domain (CRD) (SM00034); DSCAM_C - Down syndrome cell adhesion molecule C terminal (PF12355); EGF_recep_L_domain - Epidermal growth factor-like domain (SM00181); Fn2 - Fibronectin type 2 domain (SM00059); Fn3 - fibronectin type III domain (SM00060); FU - furin like repeats (SM00261); IG - Immunoglobulin domain (SM00409); Ig-like - Immunoglobulin like (SM00410); Kelch - Kelch domain (SM00612); LRR - leucine rich repeats (SM00370); PTPc - protein tyrosine phosphatase catalytic domain (SM00194); RING - ring finger (SM00184); RhoGEF - Guanine nucleotide exchange factor for Rho/Rac/Cdc42-like GTPases (SM00325); SH3 - Src homology 3 domains (SM00326); SPRY - Domain in SPla and the RYanodine Receptor. (SM00449); S_TKc - serine / threonine protein kinases catalytic domain (SM00220); WAP - four disulfide core domain (SM00217); WSC - present in yeast cell wall integrity and stress response component proteins (SM00321).

Protein	Gene	Domains	Number of contiguous FN3 domains	N-term signal peptide ?
Bent (projectin)	*bt*	IGc2, IG_like, IG, FN3, S_TKc	2, 3	N
Brother of ihog	*boi*	IG, IGc2, FN3, TM	2	Y
Contactin	*Cont*	CLECT, IGc2, IG, FN3	4	Y
domeless	*dome*	FN3, TM	5	Y
Down syndrome cell adhesion molecule	*Dscam*	IG_like, IG, IGc2, FN3, TM, DSCAM_C	4, 2	Y
Down syndrome cell adhesion molecule-2	*Dscam2*	IG_like, IG, IGc2, FN3	4, 2	Y
Down syndrome cell adhesion molecule-3	*Dscam3*	TM, IG_like, IGc2, FN3, TM	4, 2	N
Down syndrome cell adhesion molecule-4	*Dscam4*	Ig2, Ig, IGc2, FN3, TM	4, 3	Y
echinoid	*ed*	IG, IGc2, FN3, TM, TM	1	N
Eph receptor tyrosine kinase	*Eph*	EPH, FN3, EphA2, TyrKc, SAM	2	N
Fasciclin 2	*Fas2*	Ig, Igc2, FN3, TM	2	Y
FBpp0071769	*CG33143*	FN3, TM	1	Y
FBpp0075445	*CG17839*	IG, DB, FN3, IG_like, TM	1,1,2,1	Y
FBpp0077109	*CG15630*	IG, IGc2, FN3	1	Y
FBpp0077115	*CG16857*	IG, IGc2, FN3, TM	2	N
FBpp0080716	*CG10702*	EGF_Recep_L_domain, FU, FN3	2	Y
FBpp0082463	*CG3837*	EGF_Recep_L_domain, FN3	2	Y
FBpp0084049	*Wsck*	WSC, FN3, TM, S,T,Y Protein kinase	1	Y
FBpp0110105	*CG34114*	IG, IGc2, IG_like, FN3, TM	1	Y
FBpp0111687	*CG12484*	IG, Ig-like, IGc2, FN3, TM	1	Y
FBpp0112103	*CG9766*	FN3, Ank	1	N
FBpp0112375	*Unc-89*	SH3, RhoGEF, IG, IG-like, FN3, Ser/Thr/Tyr kinase	1, 1	N
FBpp0288423	*Ptp52F*	FN3, TM, PTPc	5	Y
FBpp0290384	*CG7166*	TM, IG, IGc2, FN3, TM	1	N
FBpp0293586	*CG6490*	IG_like, IGc2, IG, FN3, TM	1	Y
FBpp0293835	*CG34353*	IG, IGc2, FN3	1	N
FBpp0297247	*CG6954*	Ank, FN3, Ras associated	1	N
FBpp0297861	*CG14964*	FN3, IG	1, 1	N
FBpp0301098	*CG14372*	IG, IG_like, IGc2, FN3, TM	1	N
FBpp0301158	*CG15312*	IGc2, FN3, TM	1	Y
FBpp0301209	*CG33543*	IG, IGc2, FN3	1	Y
FBpp0304084	*CG12950*	IG, IG_like, IGc2, FN3, TM	2	Y
FBpp0305380	*CG42346*	LRR, LRR CT, FN3, TM	1	N
Frazzled	*fra*	IG, IGc2, FN3, TM, Neogenin C	6	Y
Friend of echinoid	*fred*	IG, IGc2, IG_like, FN3, TM	1	Y
Hibris	*hbs*	IG, IGc2, IG-like, FN3, TM	1	Y
Host cell factor	*Hcf*	Kelch, FN3	2	N
Insulin-like receptor	*InR*	EGF_Recep_L_domain, FU, FN3, TyrKc	3	N
Interference hedgehog	*ihog*	IG, IGc2, FN3, TM	2	Y
Kallmann syndrome 1 ortholog	*Kal1*	WAP, FN3	2	Y
klingon	*klg*	IG, IGc2, FN3	1	N
Leak	*lea*	IGc2, IG, FN3, TM	3	N
Leukocyte antigen related-like	*Lar*	IGc2, FN3, PTPc	9	Y
Miles to go (FBpp0289281)	***CG42389***	**FN3, TM**	**9**	**N**
Neuroglian	*Nrg*	IGc2, IG, IGc2, IG, FN3, TM, Bravo	5	Y
nord	*nord*	FN3	1	Y
Protein tyrosine phosphatase 4E	*Ptp4E*	TM, FN3, TM, PTPc	11	N
RIM-binding protein	*Rbp*	SH3, FN3	3	N
Roundabout	*robo*	IGc2, FN3, TM	3	N
Sallimus	*sls*	IGc2, IG, DUF1136, SH3, FN3,	1, 4	N
sevenless	*sev*	FN3, LY, TM, TyrK	1,1,2,3	N
Sidekick	*sdk*	IGc2, IG-like, FN3, TM	13	N
Sidestep	*side*	IG, IG_like, IGc2, FN3, TM	1	N
sticks and stones	*sns*	IG, IGc2, C2-set_2, FN3, TM, TM	1	N
stranded at second	*sas*	VWC, FN3, TM	3	Y
Stretchin-Mlck	*Strn-Mlck*	IG-like, IG, FN3, S_TKc	1, 1	N
Torso	*tor*	FN3, TyrKc	1	Y
Trim9	*Trim9*	RING, BBOX, BBC, FN3, SPRY	1	N
Turtle	*tutl*	IG, IGc2, FN3, TM	2	Y
Tyrosine protein phosphatase 10D	*Ptp10D*	FN3, TM, PTPc, TM	11	N

Tyrosine protein phosphatase 69D	*Ptp69D*	IGc2, IG, FN3, PTPc	3	N
Tyrosine protein phosphatase 99A	*Ptp99A*	FN3, TM, PTPc	4	Y
Wrapper	*wrapper*	IG, IGc2, FN3	1	Y

Supplemental Table 2 - Percentage of proline residues in N-terminus of FNDC3 orthologs from *Drosophila* and vertebrates.

Species	Ortholog	amino acid length(3)	% proline
D. melanogaster	*CG42389-RE*	988	8.9%
	CG42389-RF (1)	626	15.5%
	CG42389-RG	277	14.8%
M. musculus	*Fndc3a*	265	12.8%
	Fndc3b	278	13.7%
X. tropicalis	*Fndc3a*	263	14.1%
	Fndc3b	275	14.5%
G. gallus	*Fndc3a*	266	13.2%
	Fndc3b	211	14.3%
Invertebrate (2)	membrane proteins	na	3.53%
	non-membrane proteins	na	3.75%
Vertebrates (mammals) (2)	membrane proteins	na	5.68%
	non-membrane proteins	na	6.51%
Vertebrates (non-mammals) (2)	membrane proteins	na	4.53%
	non-membrane proteins	na	4.86%

Footnotes
(1) - Isoform of *CG42389* mutated in $mtgo^{e02936}$.
(2) - Data from Guar, R.K. (2014) Amino acid frequency distribution among eukaryotic proteins. *IIOABJ* **5**; 6-11
(3) - Length of N-terminus preceding first FN3 domain.

Supplemental Table 3 - Oligonucleotides used in construction of MTGO and CCT3-expression vectors

Name	Sequence (5'→ 3')[a]	Use
JB-cctγ-BamHI-s	cacgcagaaataaattaaacagccggatccatgttcggtggacag cagcca	pGEX-dmCCTγ
JB-cctγ-BamHI-as	tggctgctgtccaccgaacatggatccggctgtttaatttatttc tgcgtg	pGEX-dmCCTγ
JB-cctγ-SalI-s	ccagggtcaggagtagtagccgtcgactaaccacgtgtattaata atg	pGEX-dmCCTγ
JB-cctγ-SalI-as	cattattaatacacgtggttagtcgacggctactactcctgaccc tgg	pGEX-dmCCTγ
JB-cctγ-G297D-s	gtattcactgagaag**gat**gtctccgatctcgcc	CCTγ-G297D
JB-cctγ-G297D-as	ggcgagatcggagacatccttctcagtgaatac	CCTγ-G297D
JB-mtgo-I627TAAstop-s	ccatctgctccgcctcca**taa**cattgcagtgatc	MTGO(1-626)
JB-mtgo-I627TAAstop-as	gatcactgcaatgttatggaggcggagcagatgg	MTGO(1-626)
JB-mtgo-P1021TAAstop-s	atcgcgagaacagcatcattgagcaa**taa**tcagctattgaaaaac ctg	MTGO(1-1020)
JB-mtgo-P1021TAAstop-as	caggtttttcaatagctgattattgctcaatgatgctgttctcgc gat	MTGO(1-1020)
JB-mtgo-S1561TAAstop-s	ccagtgaactggatcctagc**taa**gcgacctgtc	MTGO(1-1560), MTGO(620-1560)
JB-mtgo-S1561TAAstop-as	gacaggtcgcttagctaggatccagttcactgg	MTGO(1-1560), MTGO(620-1560)
JB-mtgo-A1739TAAstop-s	cgtcttagcgaccaacaaaag**taa**gtgtgcattgtggtctccttc	MTGO(1-1738), MTGO(620-1738)
JB-mtgo-A1739TAAstop-as	gaaggagaccacaatgcacacttacttttgttggtcgctaagacg	MTGO(1-1738), MTGO(620-1738)
JB-mtgo-*Nco*I-474-s	actcacacgcccactcgccc**atg**gctccccagccacatgcaca	MTGO(474-1738)
JB-mtgo-*Nco*I-474-as	tgtgcatgtggctggggagccatgggcgagtgggcgtgtgagt	MTGO(474-1762)
JB-mtgo-*Nco*I-620-s	ccggcgatgatgaggaggagtaccc**atg**gagaacagcatcattg agcaaatc	MTGO(620-1762), MTGO(620-1738), MTGO(620-1560)
JB-mtgo-*Nco*I-620-s	gatttgctcaatgatgctgttctccatggggtactcctcctcatc atcgccgg	MTGO(620-1762), MTGO(620-1738), MTGO(620-1560)

[a]Introduced *BamH*I, *Sal*I, and *Nco*I restriction sites used for cloning are underlined. The mutagenized codon for the G297D change is shown in bold. Introduced start and stop codons are also shown in bold.